LAYER-BY-LAYER ASSEMBLY OF THIN PLATELET-POLYMER CONDUCTIVE BARRIER FILMS

A Dissertation

by

BARTON EMORY STEVENS

Submitted to the Office of Graduate and Professional Studies of
Texas A&M University
in partial fulfillment of the requirements for the degree of

DOCTOR OF PHILOSOPHY

Chair of Committee,	Jaime Grunlan
Committee Members,	Terry Creasy
	Donald Darensbourg
	Miladin Radovic
Head of Department,	Andreas Polycarpou

May 2015

Major Subject: Mechanical Engineering

ABSTRACT

A wide assortment of properties can be achieved in polymer nanocomposites prepared using layer-by-layer assembly. Through aqueous processing in ambient conditions, thin film gas barriers and electrical conductors, for example, can be made to rival films created by more arduous processing techniques, such as vacuum deposition. In this work, polymer/platelet nanocomposite thin films were studied. Montmorillonite clay (MMT) was deposited with pyrene-labeled polyethyleneimine (PEI-Py), which was synthesized and used for its ability to partially self-agglomerate when deposited. This led to denser deposition of layers, allowing the role of density in thin film gas barriers to be probed. Increased density (1.45 vs. 1.24 g/cm^3 for neat PEI films) led to a drastic increase in barrier properties (0.059 vs. 0.75 cm^3/m^2/day/atm) for films of similar thickness (after 12 deposition cycles). When graphene oxide (GO) and PEI were layered and thermally reduced, electrical conductivity (1750 S/m) resulted. Undectable (< 0.005 cm^3/m^2/day/atm) oxygen barrier of GO-based films was realized after ≤ 20 deposited layers in low humidity conditions. At high humidity, films containing reduced GO were more than 100x more effective at blocking O_2. These same films were patterned before reduction to form conductive pathways. Patterning was accomplished by exposing the films to a basic solution absorbed in patterned agarose stamps. This wet etching technique was used to remove the GO-based assembly quickly, and SEM confirmed that little material was left behind after etching. GO charge, layer thickness, and resistivity are closely related to pH. As the pH decreases, GO particles become more neutral in solution, confirmed by lower zeta potential, leading to thicker deposition and lower resistivity.

NOMENCLATURE

BL	Bilayer
EDS	Energy dispersive x-ray spectroscopy
FIB	Focused Ion Beam
FT-IR	Fourier transform infrared spectroscopy
GO	Graphene oxide
LbL	Layer-by-layer
MMT	Sodium montmorillonite clay
OTR	Oxygen transmission rate
PAA	Poly(acrylic acid)
PAH	Poly(allylamine hydrochloride)
PEI	Polyethyleneimine
PEI-Py	Pyrene-labeled polyethyleneimine
PET	Polyethyleneterephthalate
PSS	Poly(styrene sulfonate)
QCM	Quartz crystal microbalance
QL	Quadlayer
rGO	Reduced graphene oxide
RH	Relative humidity
SEM	Scanning electron microscopy
TEM	Transmission electron microscopy
XPS	X-ray photoelectron spectroscopy

TABLE OF CONTENTS

Page

LIST OF FIGURES

FIGURE Page

LIST OF TABLES

TABLE Page

I. INTRODUCTION

1.1 Background

Strong interest in traditional and flexible organic electronics is driving the need for electrically conductive layers with high oxygen barrier properties that can be applied using low cost methods.[1] With growing interest in flexible electronics, finding equally flexible materials that can adapt to these purposes is a necessity. Organic light emitting diodes (OLEDs), for instance, become inoperable within hours of exposure to oxygen and water vapor.[2,3] Commercially available options that meet these requirements rely on expensive vapor phase application under vacuum,[4] such as SiO_x, Al_xO_y, and metallized films, which are subject to cracking under strain and suffer from pinhole defects.[5–10] The expense and rigidity of these coatings makes them poor candidates for the protection of OLEDs, so other types of encapsulation will be necessary for their commercialization. Both clay and graphene oxide offer considerable advantages in this regard, as both are relatively inexpensive and graphene oxide is water-dispersible. Graphene oxide can also be reduced into an electrically conductive form.[11]

Patterned conductive surfaces are ubiquitous in electronic devices, being commonly utilized in printed circuit boards (PCBs) and integrated circuits (ICs). Traditional PCB and IC designed around rigid substrates—epoxy for PCBs and silicon/silicon dioxide for ICs—in their manufacture. These rigid substrates are unsuitable for flexible electronics. Furthermore, the fabrication of these patterned surfaces is both complicated, expensive, and dangerous.[12] PCB patterning uses either electroplating or electroless plating, both of which produce a considerable amount of toxic side products and environmental pollutants.[13,14] IC fabrication, through commonly-

used photolithography, results in a large number of contaminants from chemicals used to treat wafers.[15,16] Patterning of conductive pathways on flexible substrates is impossible using these current technologies, though both would benefit substantially from simplified environmentally-friendly techniques.

Both patterning of circuits and gas barrier packaging for electronics can be much safer and less expensive if durable electrically conductive coatings can be applied from aqueous solutions of benign chemicals and processed under ambient or near-ambient conditions. In the present work, layer-by-layer (LbL) processing was used to achieve this goal. LbL processing, a method whereby substrates are dipped into alternate solutions of aqueous polyelectrolytes, as shown in Figure 1.1, produces a thin (typically < 1 µm) coating[17–19] capable of applications as diverse as drug delivery,[18,20–22] sensing,[23,24] self-cleaning,[25,26]and flame retardancy.[27,28] The thickness and morphology of the deposited layers may be tuned by varying processing conditions (e.g. pH[29] and concentration[30]) of the requisite solutions, which ultimately influences macroscopic properties, such as gas permeability.[31–33] When graphene oxide is incorporated into these films, gas barrier and electrical conductivity are attainable.[34,35] LbL processing with graphene oxide (GO) and polyethyleneimine (PEI) is able to realize coatings that are both impermeable to gas and electrically conductive. Preliminary results show that layers formed with these materials are capable of ultra-low gas permeability (below 7×10^{-22} cm^2/s/Pa on PET film) with conductivity of 1750 S/m.

1.2 Objectives and Dissertation Outline

The purpose of the research contained herein is to explore the multi-functional nature of polyelectrolyte multilayer assemblies, specifically oxygen barrier and electrical conductivity. This research is ultimately important to electronics, which are

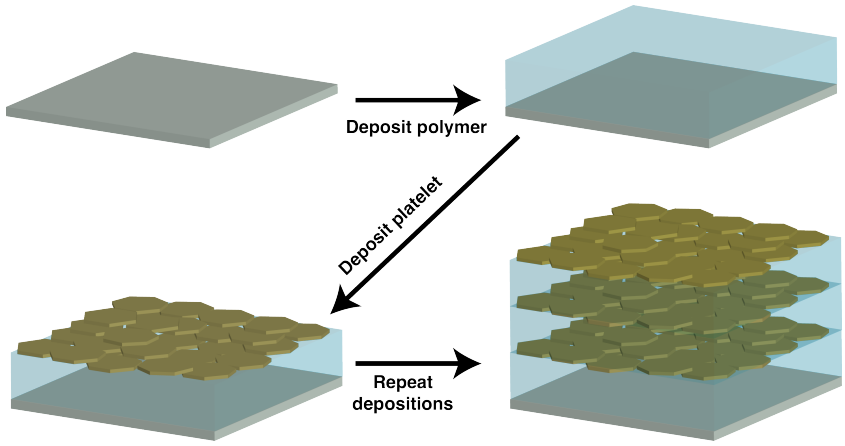

Figure 1.1: Schematic of layer-by-layer growth of polymer and platelet polyelectrolytes. The polymer is deposited, followed by rinsing, then the platelet is deposited followed by another rinse. This process is repeated until the desired number of layers is deposited.

in need of both barrier films (to protect susceptible organic components within) and conductive films (as antistatic layers and electrodes). This work presents proof of concept for multilayer films containing nanoplatelets (clay, graphene oxide).

Chapter II presents a review of layer-by-layer technology, gas barriers, and graphene oxide. Layer-by-layer is a processing technique that was used to deposit polyelectrolytes onto surfaces for every study in this dissertation. An overview of permeation and theories surrounding how gas molecules diffuse in polymer multilayers is also presented, along with a summary of existing barrier films. Graphene oxide (GO) is also surveyed because it is only recently beginning to find extensive use in materials and because the chemistry, structure, and uses of this material is not yet commonplace.

Chapter III describes thin film assemblies made from a chemically-modified polyelectrolyte. In this study, polyethyleneimine (PEI) was labeled with pyrene groups, which are known to have π-π stacking interactions with itself and other conjugated materials. This hydrophobic interaction causes the polymer to coil in solution with-

out completely losing water solubility. This polymer was compared with neat PEI in clay-containing assemblies with regard to film thickness, density, and oxygen barrier properties. Fourier-transform infrared spectroscopy (FTIR) was used to determine effectiveness of pyrene labeling. Film density was calculated from quartz crystal microbalance (QCM) and profilometry measurements, which measure mass deposited and thickness, respectively. Oxygen transmission rate (OTR) testing was performed to determine the permeability of these assemblies.

Chapter IV describes how reduction of GO in GO/PEI influences gas barrier properties and imparts electrical conductivity. GO before and after reduction in the already-deposited assemblies was investigated by reducing with heat above 150°C. The reduction was monitored through x-ray photoelectron spectroscopy and electrical conductivity measurements. The resulting microstructures were analyzed by both scanning and transmission electron microscopy. The oxygen barrier of the film, in both dry and humid environments, was shown to be influenced by the reduction.

Chapter V examines using the same films described in Chapter IV for patterning using wet stamping. In this study, films were deposited and selectively etched by swelling agarose stamps with basic solutions, which was effective in removing exposed film. The effect of changing the pH of GO suspensions was also evaluated to determine if thickness of the films would have an influence on conductivity and etch. The influence of pH on GO suspensions was monitored by zeta potential measurements, while the film thickness was determined by profilometry and conductivity by a four-point probe apparatus. The quality of the etch was examined by energy-dispersive x-ray spectroscopy (EDS) mapping, SEM, and FTIR.

Chapter VI looks at the overall impact of this work and possible future directions. The dissertation was focused on gas barrier and electrical conductivity of multilayer assemblies. To further improve upon these systems, refinement of patterning tech-

niques, such as photolithography, will need to be employed along with inclusion of other conductive fillers to replace electrically-insulating PEI. Decreasing feature size of patterned films will increase their attractiveness for use in commercial electronics.

II. LITERATURE REVIEW

2.1 Layer-by-Layer Assembly

2.1.1 Parameters Influencing Assembly

The processing technique that is known today as layer-by-layer (LbL), and used to form polyeletrolyte multilayers (PEMs), was first described by Iler in 1964. Iler initially studied the mutual adsorption of colloidal silica onto alumina and colloidal alumina onto silica. He noted several important factors: (1) controlling solution pH in these experiments in order for siliceous substrates to bear a negative charge, which would attract a monolayer of alumina and reverse the charge on the surface, (2) the attracted species must be present in excess in order to fully reverse the surface charge, and (3) coatings made using this technique did not easily rinse off.[36] In 1966, Iler developed the first multilayers using alumina fibrils and spherical silica particles to coat black glass by dipping the glass into one solution, carefully rinsing and drying the glass to remove excess colloidal particles, and dipping into the other solution and rinsing. Repeating this process of dipping, he was able to increase the thickness of the adsorbed layers to produce films on the order of 100 to 1000 µm.[37]

In 1992, Decher introduced LbL processing with polymer polyelectrolytes. With polystyrenesulfonate (PSS), polyvinylsulfate, poly(allylamine hydrochloride) (PAH) and poly(4-vinylbenzyl-(*N*,*N*-diethyl-*N*-methyl-ammonium iodide), it was shown that consecutive submersions of silicon or quartz in alternately charged solutions produced multilayers on the substrate. Figure 2.1 shows a schematic of this process. Monitoring the film thickness by small angle x-ray scattering and UV/vis spectroscopy, it was shown that the thickness of the films corresponded directly with the number of deposited layers.[17,38,39]

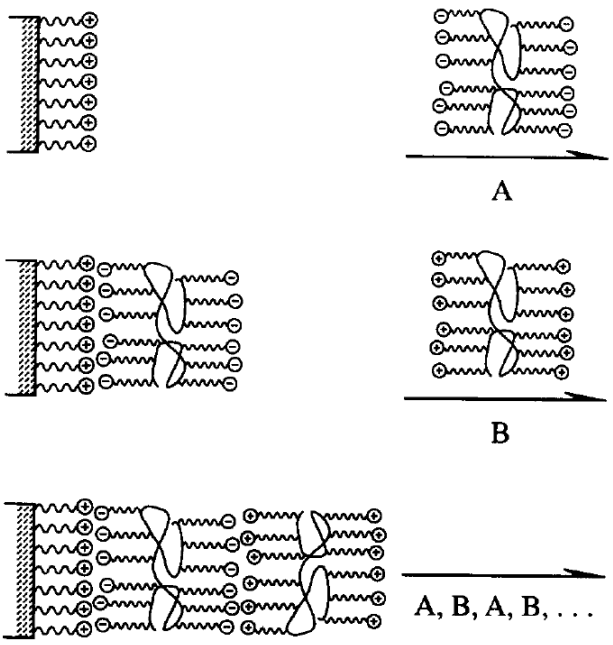

Figure 2.1: Schematic of layer-by-layer growth of polymer polyelectrolytes. After each consecutive dip into aqueous solution, the charge on the surface is reversed. This process can be continued to produce an arbitrary number of layers. Adapted from ref. [39].

The microstructure of these films was investigated to determine whether discrete layers existed. With x-ray data alone, it was impossible to tell whether the layers were discrete (they were too close to yield enough contrast), so neutron scattering was employed. When every polyanion layer was deuterium-labeled, neutron scattering also displayed an absence of Bragg peaks, indicating that the polyelectrolyte layers overlap considerably. This led to the conclusion that the concentration profile of each layer in the film must overlap considerably with the layer on either side of it, as shown in Figure 2.2.[40]

For polyelectrolyte multilayer assembly, a number of factors determine how the film will grow. Weak polyelectrolytes, those with pK_a values in the range of 0-12, have charge and conformation characteristics governed primarily by solution pH.

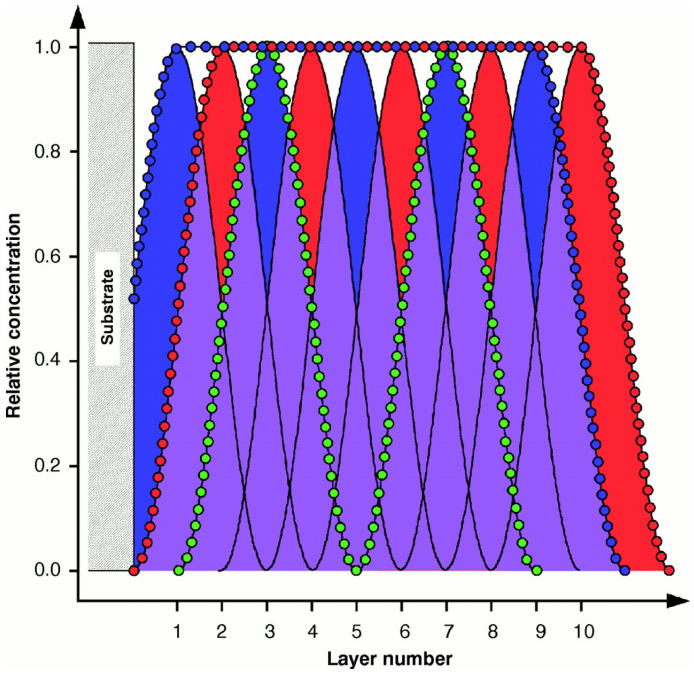

Figure 2.2: Schematic of layer-by-layer growth of polymer polyelectrolytes. After each consecutive dip, the charge on the surface is reversed. This process can be continued to produce an arbitrary number of layers. Adapted from ref. [40].

For instance, when a polyacid is in solution at low pH, it is mostly protonated and uncharged, and it will adopt a coiled solution conformation. At high pH, this same polymer it is mostly deprotonated, highly charged, and extended in solution. The polymer conformation leads to increased (uncharged, coiled) or decreased (charged, extended) layer thickness. If both polyelectrolytes used in the LbL process (one polyacid and one polybase) are adjusted to the same pH conditions, a maximum in thickness will be observed when both polymers have lower charge density in neutral pH conditions.[30,41] Increasing the ionic strength by adding salt to polyelectrolyte solutions causes their charge to be screened. This causes them to adopt more coiled conformations, the extent of which is controlled by the salt concentration and valency. The resultant increase in thickness is proportional ionic strength as I^a, where I is the

ionic strength and a ranges from 0.5 to 1.[42–44] Increasing the temperature of solutions for LbL assembly causes additional swelling in most polyelectrolytes, which causes greater interpenetration of layers and leads to increased thickness (Figure 2.3).[45–47]

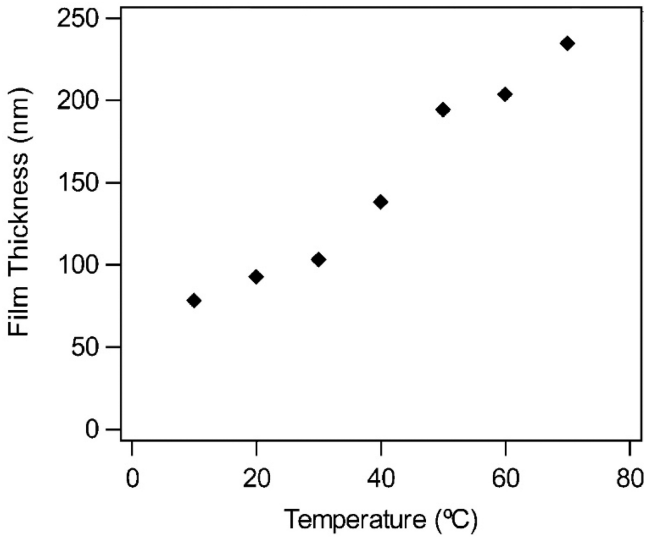

Figure 2.3: Film thickness as a function of deposition temperature. Thicker films result from increasing temperature due to increased entanglement of the depositing species with the already-deposited film. Adapted from ref. [47].

Though electrostatic interactions are the most common in LbL processing, many other interactions can be employed, several of which preclude the need for polyelectrolytes altogether.[48] Hydrogen-bonded assemblies have been used for polymers with low charge density or non-polyelectrolyte polymers, such as poly(ethylene oxide), poly(vinyl alcohol), polyvinylpyrrolidone, and even biological macromolecules such as proteins and DNA.[49–53] Charge transfer interactions between donors and acceptors have also been demonstrated in multilayer films. In this type of interaction, a charge donor on one polymer forms a complex with an acceptor on another,

which has been shown between a carbazole and a nitrobenzoyl.[54,55] Binding is also possible between different species through biological interactions, such as antibody-antigen and avidin-biotin conjugation.[56,57] Inorganic complexation–interactions between metal centers and ligands–leads to the formation of extended networks, which can be built into a surface coating. For example, Zr(IV) can bind to four separate 1,10-decanebisphosphonate molecules, which can themselves bind two Zr each.[58] In another study, PSS sodium salt was cation exchanged with Cu^{2+} and layered with polyvinylpyrrolidone, which acts as a ligand to the copper centers.[59] Forming covalent linkages between layers in these LbL assemblies is another approach, which can involve many different organic bond-forming reactions. In many cases, these films are more robust to mechanical and chemical attack.[60–62]

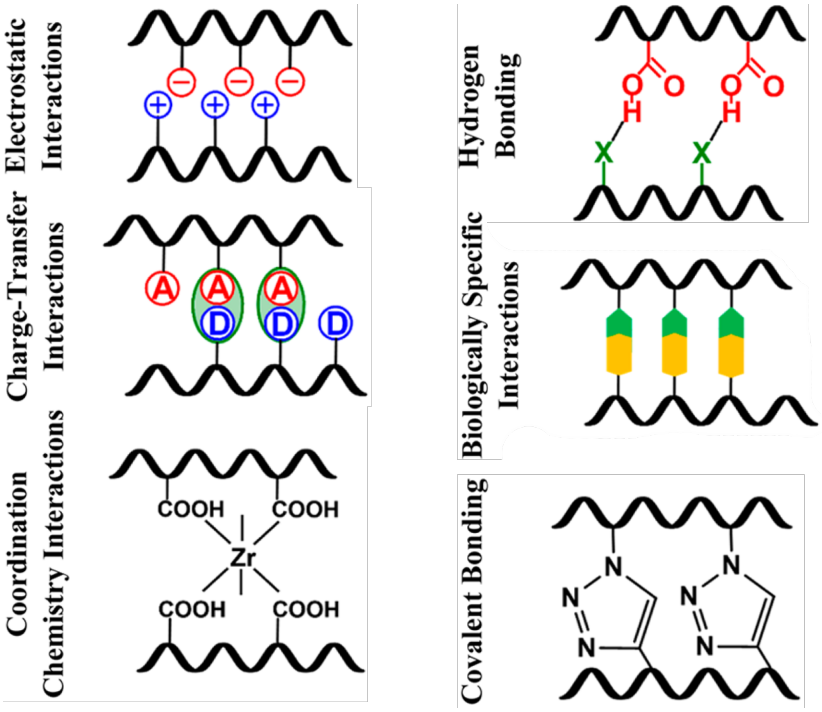

Figure 2.4: Types of interactions suitable to produce LbL films. Adapted from ref. [48].

2.1.2 Applications

Layer-by-layer deposition has been used extensively for the wide variety of properties it can impart. These properties serve roles in nearly every area of science and engineering, including biology and biomedical engineering, chemistry and chemical engineering, energy, electrical engineering, and others. The relative ease of processing (typically in ambient conditions with water as a solvent) makes it an attractive technology.

Biological and biomedical engineering applications of LbL are among the most popular uses for this technique.[63] Onda investigated anionic glucose oxidase layered with several different polycations, which produced films containing the enzyme. The films exhibited catalytic activity, converting O_2 and glucose into H_2O_2, which was maintained for weeks after storage in air and treatment of the films with various pH and temperature conditions.[64] Peroxidase has also been used in similar films to convert the products of glucose oxidase catalysis into water, while monitoring an indicator dye DA67. Monitoring the conversion spectroscopically, it was found that increasing the number of layers increased the rate of conversion.[65] Glucose oxidase-containing assemblies are also good glucose detectors, with detection limits as low as 0.20 mmol/L.[66] Other biosensors are also possible, such as layered anti-IgG being capable of detecting IgG.[67]

Because polyelectrolyte-based assemblies are pH sensitive, they are easily used for pH stimulated release of therapeutics. Layering PAH and sodium hyaluronate and soaking the films in Indoine blue or Chromotrope 2R, both commercial dyes, Burke showed that the dyes could diffuse into the films. Deswelling the films was easily achieved by monitoring UV/vis spectra after immersing the dye-swollen films in solutions of various pH. The exact pH of maximal deswelling dependeds on the

dye (Figure 2.5).[68] Heparin and chondroitin sulfate, actual chemical therapeutics, display similar behavior.[69]

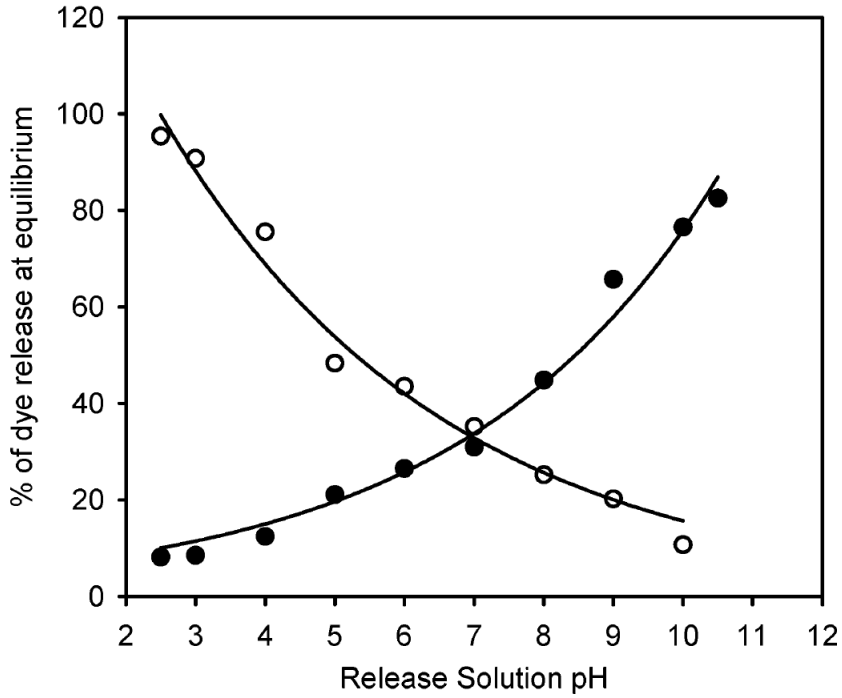

Figure 2.5: Release of Chromotrope 25 (filled) and Indoine Blue (unfilled) as a function of pH from PAH/hyaluronate films swollen with the dyes. Adapted from ref. [68].

Multilayer films have also been used extensively to solve traditional chemical engineering challenges.[70] Gas separation, especially for light gases such as H_2, CH_4, N_2, CO, and CO_2, is of particular interest. McCarthy showed excellent selectivity (> 100) for H_2/N_2 using PAH/PSS multilayer films, with selectivity increasing, but permeation decreasing, with the number of deposited layers.[71] Sullivan coated poly(amic acid)/PAH on porous alumina, which was then heated to convert poly(amic acid) into polyimide. This coating provided selectivity of 6.9 for O_2/N_2

and 68 for CO_2/CH_4, with relatively high permeability.[72] Applying polyethyleneimine (PEI) and poly(acrylic acid) (PAA), Kim was able to not only exceed the Robeson upper bound, recreated in Figure 2.6, but achieve selectivities greater than any ever reported for both H_2/CO_2 and H_2/N_2 separation.[73] Gas barrier has also been studied extensively, which will be the topic of later chapters, but PEI/montmorillonite (MMT), PEI/PAA, and PEI/PAA/PEI/MMT have all been shown to reduce O_2 permeation on PET by 3-4 orders of magnitude.[74–76] Reverse osmosis with LbL films has also been studied. Layering polyvinylamine and poly(vinyl sulfate potassium salt) on polyacrylonitrile (PAN)/PET substrates resulted in salt rejection for NaCl and Na_2SO_4 of up to 93.5% and 98.5%, respectively.

Applications of LbL to electronics are vast. Nanoparticle incorporation, for instance, is popular for making electrically conductive films. Carbon nanotubes have been used to make conductive thin films through either covalent functionalization or stabilization by surfactants or polymer. Such systems include carboxyl- and amine-functionalized CNT layers, PDDA/CNT from multi-walled CNTs stabilized in borate buffer, and PDDA/CNT from single-walled CNTs stabilized with deoxycholate..[77–79] Many novel materials have been used to create devices as well. Kovtyukhova fabricated p-n heterojunction diodes from a double-layered LbL film of n-type $W_{12}O_{41}/TiO_2$ on top of p-type PAN/CNTs.[80] Dye-sensitized solar cells were fabricated by layering PDDA and TiO_2, which was then loaded with a ruthenium dye by Agrios, which was capable of $> 5\%$ efficiency.[81] Electrochromic response has even been observed by Park in films containing poly(vinyl pyridine-co-styrene) and WO_4^{2-}, shown in Figure 2.7.[82]

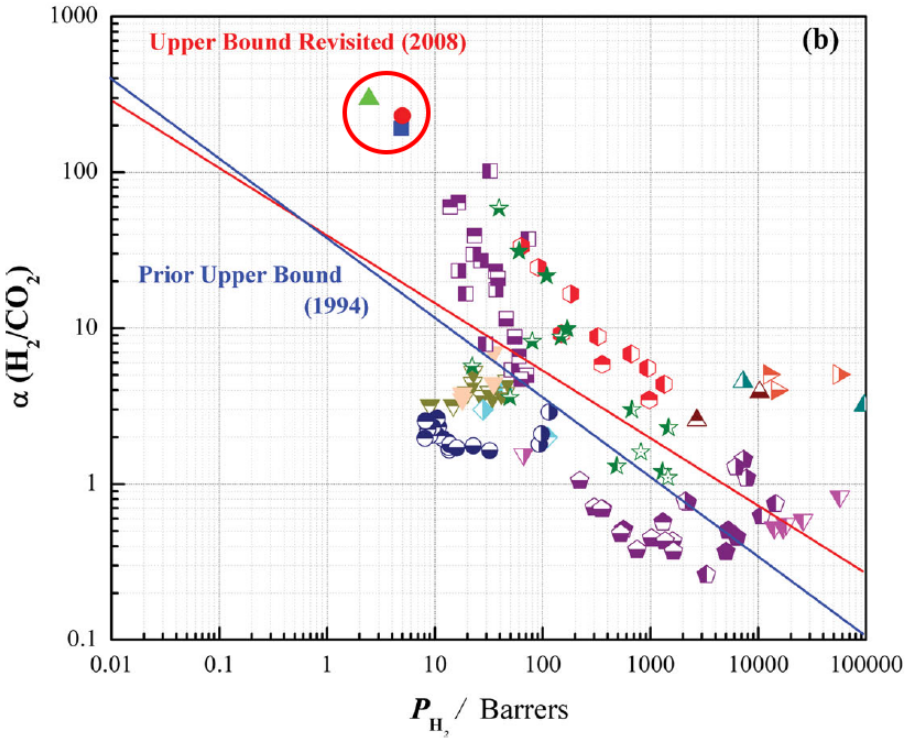

Figure 2.6: Robeson upper bound plot for H_2/CO_2 selectivity as a function of H_2 flux. PEI/PAA multilayers (circled in red) display better selectivity than any other material, including metal-organic frameworks and zeolites. Adapted from ref. [73].

2.2 Gas Barriers and Diffusion

2.2.1 Gas Barriers

Gas barriers are of particular interest in packaging, as barriers are needed to keep unwanted gases (typically O_2 and H_2O) from interacting with the contents. As Table 2.1 shows, this is not a trivial problem because polymer permeability is high to most common gases.[83,84] LDPE and PET are inexpensive and flexible packaging materials, some kind of treatment must be performed so that shelf life of the packaged good (food, e.g.) can be extended as far as possible.

Since the 1970s, metallization has traditionally imparted excellent barrier prop-

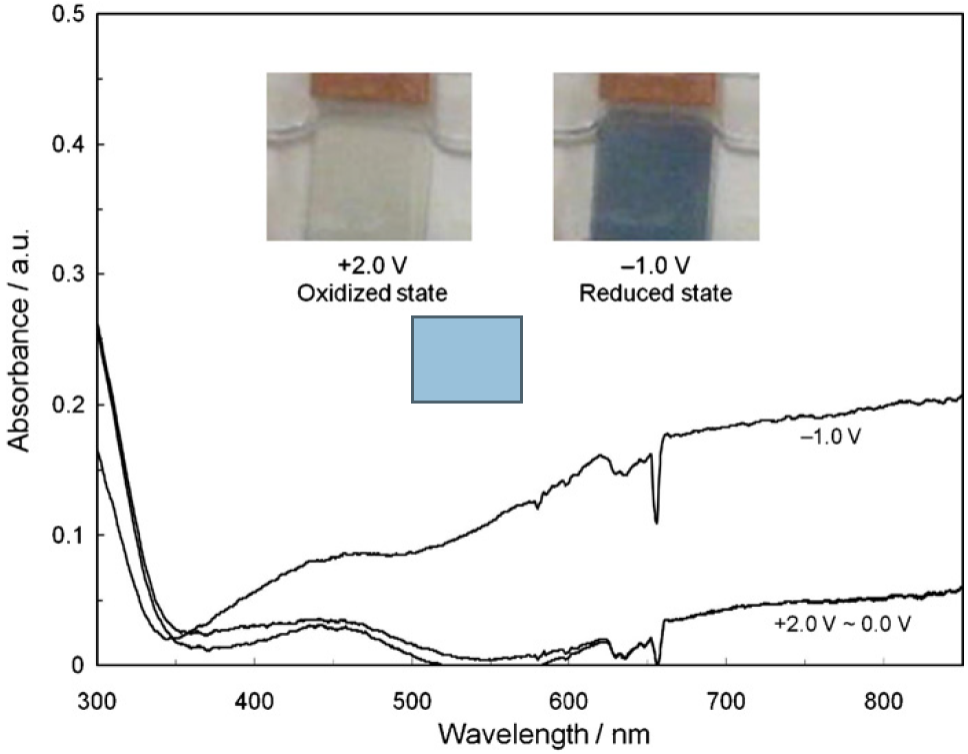

Figure 2.7: Electrochromic response of WO_4^{2-}-based LbL films. Adapted from ref. [82].

erties to polymer packing materials.[85,86] Metallized polymers typically offer several orders of magnitude in reduction in oxygens permeability. Polymer films are typically metallized in vacuum in a roll-to-roll scheme in which hot metal in crucible is evaporated onto the polymer film as it passes over in the process of spooling the film from one roll to another, as illustrated in Figure 2.8. This process results in a uniformly-coated barrier film that reduces O_2 permeation by two orders of magnitude,[83,85,86] metallization has three main drawbacks: vacuum is industrially expensive and difficult maintain, it is not microwavable, and it is completely opaque.

In response to the shortcomings of metallized films, SiO_x coatings were developed in the 1980s for transparent barrier layers on polymer films.[85,87,88] Plasma-enhanced

Table 2.1: Permeability of common polymers to O_2 and H_2O Adapted from ref. [83].

Polymer	Oxygen Permeability at 23 °C, 50% or 0% RH [$cm^3mm/m^2/day/atm$]	Water vapour permeability at 23 °C, 85% RH [$g \cdot mm/m^2/day$]
Poly(ethylene terephthalate) (PET)	1-5	0.5-2
Polypropylene (PP)	50-100	0.2-0.4
Polyethylene (PE)	50-200	0.5-2
Polystyrene (PS)	100-150	1-4
Poly(vinyl chloride) (PVC)	2-8	1-2
Poly(ethylene naphthalate) (PEN)	0.5	0.7
Polyamide (PA)	0.1-1 (dry)	0.5-10
Poly(vinyl alcohol) (PVAL)	0.02 (dry)	30
Ethylene vinyl alcohol (EVOH)	0.001-0.01 (dry)	1-3
Poly(vinylidene chloride) (PVDC)	0.01-0.3	0.1

chemical vapor deposition (PECVD) is typically used to deposit SiO_x on plastic substrates from the reaction of precursor silane and oxygen gases. If the gas ratio is not carefully controlled in this process, atomic oxygen (formed in the plasma) is capable of etching holes in the polymer film.[89] These coatings provide similar barrier characteristics, but unlike metallized film, they are tranparent and microwavable. Like metallized films, however, SiO_x is also applied under vacuum and it suffers from another major limitation—SiO_x is subject to cracking (Figure 2.9)—which negates its barrier properties.[6,87]

Simpler and more cost-effective polymer processing techniques, such as co-extrusion or co-injection, are possible with bulk polymer composites. Polypropylene/ethylene vinly alcohol and poly(ethylene terephthalate)/liquid crystal polymer blends and epoxy/clay composites, for instance, are capable of reducing permeability by an order of magnitude.[83,90–92] Although processing is much simpler for these materials,

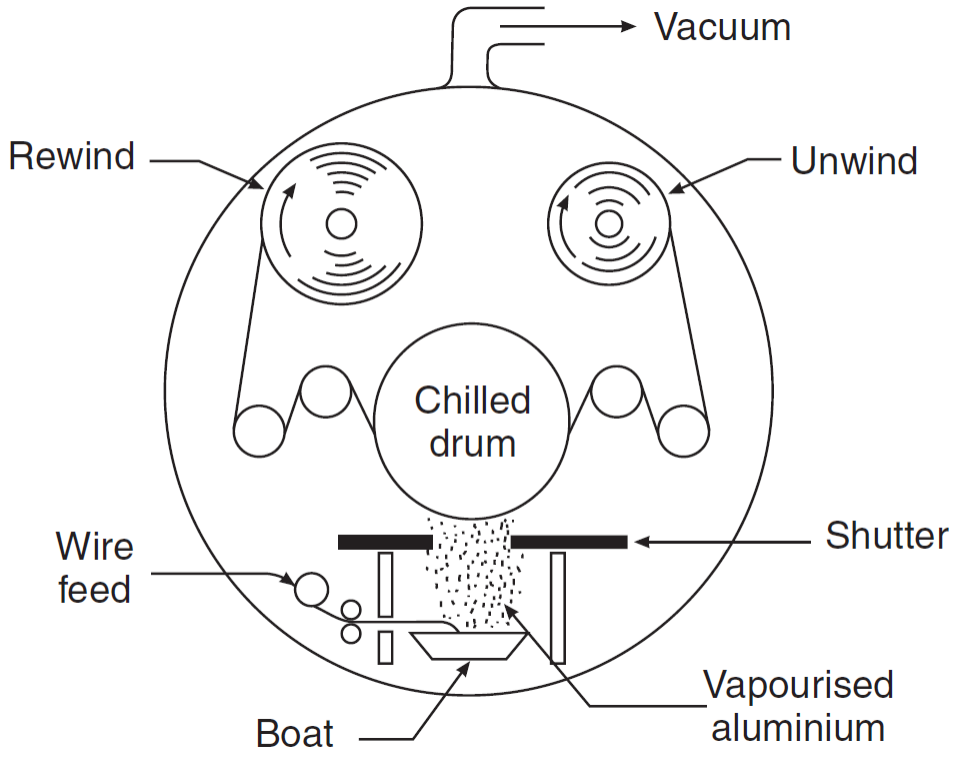

Figure 2.8: Roll-to-roll processing of polymer film in vacuum by passing continuously fed film over evaporating aluminum. Adapted from ref. [86].

the oxygen barrier achieved is typically worse than metallization or SiO_x can achieve (by an order of magnitude or more). Additional difficulties in producing complete blends and adequate dispersions, which effect mechanical and visual properties, are also challenges.

2.2.2 Gas Diffusion

In uniform, homogeneous solids at steady state, Fick's Law (Eq. 2.1) relates the diffusive flux J (the amount of diffusing species per area per time) to the diffusion coefficient D (generally proportional to an Arrhenius expression and specific to diffusing species and the material through which diffusion is occurring), the con-

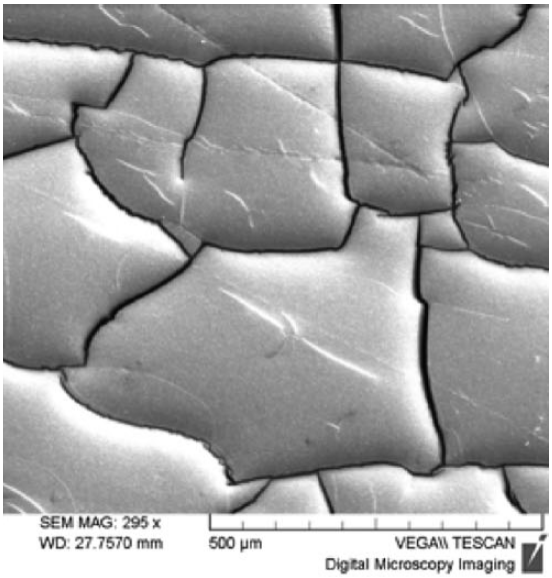

Figure 2.9: Scanning electron micrograph of cracked SiO_x on polypropylene. Adapted from ref. [87].

centration of the diffusing species ϕ, and position x. For barrier materials, this expression produces a relationship between the gas flux, diffusivity in the material, and the concentration of the gas in the material at a given depth:[93]

$$J = -D\frac{\partial \phi}{\partial x} \tag{2.1}$$

For thin films, the gas generally diffuses through the entire film, and Fick's law can be expressed as:

$$J = -P\frac{A\Delta p}{t} \tag{2.2}$$

In this case, J is related to the film area A and thickness t, permeability coefficient P (analogous to the diffusivity coefficient) and pressure drop across the film Δp.[94] For thin barrier coatings on substrates, ideal laminate theory can be used to determine

the overall permeability of a film based on the permeability of the component layers:[7]

$$P = \left(\frac{t_c}{P_c t} + \frac{t_s}{P_s t} \right)^{-1} \tag{2.3}$$

Similar to electrical resistors in parallel, the reciprocal of the overall film permeability P is the sum of the reciprocal of the coating permeability P_c and substrate permeability P_s, which are both scaled by their relative thicknesses $\frac{t_c}{t}$ and $\frac{t_s}{t}$. In the research presented in this dissertation, Equation 2.3 is used to calculate the P_c, as P and P_s are found experimentally through gas transmission testing.

2.2.3 Nielsen Model

Fickian diffusion is not possible for materials with heterogeneous microstructures, as diffusion through the components of the material differs. The simplest way to model behavior in nanocomposite films is to consider the nanocomposite as a binary mixture of gas-permeable and gas-impermeable components. In polymer nanocomposites, the polymer is most often both the continuous and permeable phase. Common impermeable materials include ceramic oxides, clays, and carbon nanomaterials.[34,76,92,95–99] As illustrated in Figure 2.10, incoming gas molecules are forced to diffuse around impermeable flakes, leading them to take a long path through the material that increases diffusion time. A few models have been proposed to explain the effects these fillers have on gas diffusion in polymer composite thin films.

Nielsen made the earliest attempt at explaining the barrier behavior of nanocomposite thin films in 1967, suggesting ideal behavior of flake-like fillers that are uniform in size and all oriented perpendicular to the diffusion direction in a regular array.[95,100,101] The filler particles are completely dispersed in the matrix, and effects of voids, poor dispersion, and misaligned particles that would adversely affect barrier

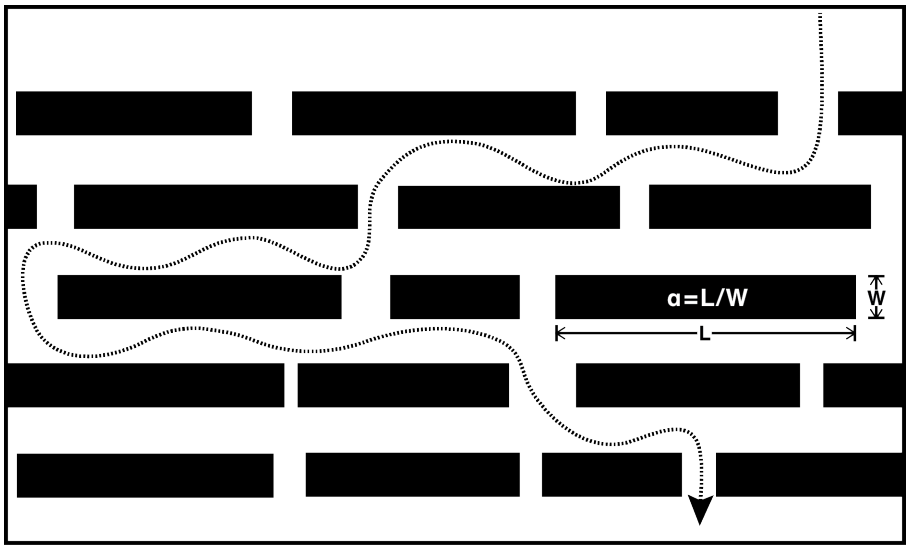

Figure 2.10: A schematic of gas diffusion through a polymer film containing impermeable flakes. Incoming gas molecules are incapable of taking a direct route, so a more tortuous path is taken, leading to increased diffusion time. A typical flake is characterized by its aspect ratio α (its length divided by its width).

properties are not considered. The relative permeability is given by:

$$\frac{P}{P_0} = \frac{1 - \Phi}{1 + \frac{\Phi\alpha}{2}} \tag{2.4}$$

where P is the composite permeability, P_0 is the permeability of the neat polymer, Φ is the volume fraction of filler, and α is the aspect ratio of the filler particle. The effect of aspect ratio is shown in Figure 2.11.

The basis for decreased permeation in the Nielsen model is increased path length of gas molecules due the tortuosity of the composite: volume fraction of filler and particle aspect ratio are the only factors governing gas permeation. This model provides a good theoretical basis for flake-filled polymer composites, but is unable to account for such factors as non-perpendicular orientation and polydispersity of the

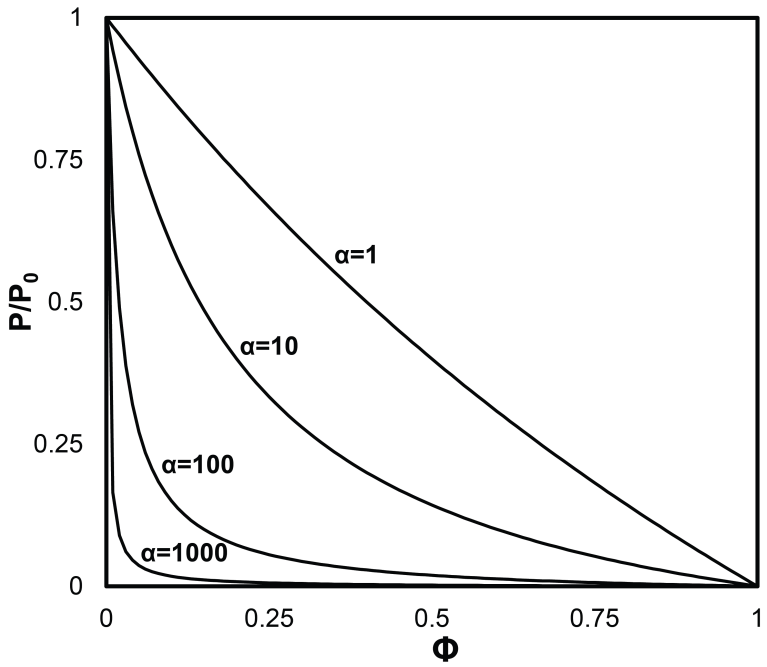

Figure 2.11: Plot of relative permeability as a function of volume fraction of filler, with various aspect ratios in polymer composite films, according to the Nielsen model. Adapted from ref. [100]

particles and fails to distinguish one-dimensional filler particles (such as rods) from two-dimensional filler particles (such as platelets).

2.2.4 Cussler Models

In 1988, Cussler proposed a model that addresses deficiencies in the Nielsen model, and refinements of this model continue to be made for various fillers.[102–104] Similar to the Nielsen model, the Cussler model considers the diffusing species to be taking a toruous path between impermeable flake fillers, and that the barrier properties are driven entirely by lengthening of the diffusion path. The first notable difference between the Cussler and Nielsen models is that the Cussler model considers the spacing between particles in a regular array σ, from which the predicted

relative permeability is derived:

$$\frac{P}{P_0} = \left(1 + \frac{\alpha\Phi}{\sigma} + \frac{\alpha^2\Phi^2}{1-\Phi}\right)^{-1} \tag{2.5}$$

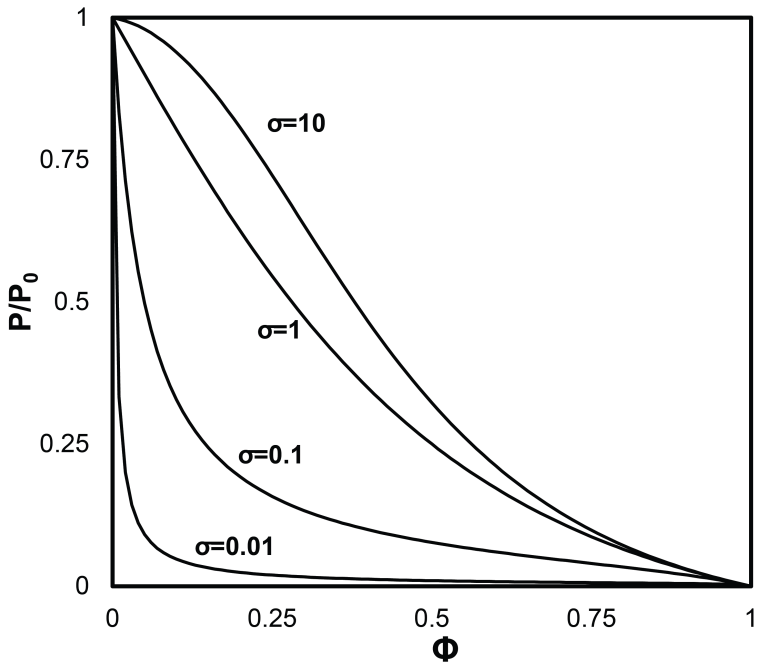

Figure 2.12: Plot of relative permeability vs. volume fraction of filler with various pore spacings in polymer composite films according to the Cussler model.[102] A constant $\alpha = 2$ is used.

Figure 2.12 illustrates the relationship between decreasing σ and decreasing relative permeability. For irregularly-spaced arrays of particles, Cussler also provided a generic basis for the determination of relative permeability based on a geometric factor μ:

$$\frac{P}{P_0} = \left(1 + \mu\alpha^2\left(\frac{\Phi^2}{1-\Phi}\right)\right)^{-1} \tag{2.6}$$

Initially, μ was not assigned a particular value, but later refinements to the model were made to account for this:

$$\frac{P}{P_0} = \left(\frac{\left(1 + \frac{2}{3}\alpha\Phi\right)^2}{1 - \Phi} \right)^2 \tag{2.7}$$

Further adjustments to the Cussler model have also explained how polydispersity in the particle size distribution affects permeability.[103]

2.2.5 Other Barrier Models

While the work of Nielsen and Cussler has provided a strong foundation for the description of gas permeation in flake-filled polymer composites, other notable models have also been generated. These include the developments of Bharadwaj,[105] Fredrickson and Bicerano,[106] and Gusev and Lusti,[107] each of which addresses complexities not previously considered.

The Bharadwaj model considers the case for which particles are not aligned perpendicular to the direction of permeation. This was accomplished by introducing a shape factor S (Eq. 2.8) to account for various rotations of platelets θ, where $\theta = 0$ indicates perpendicular alignment and $\theta = \frac{\pi}{2}$ indicates parallel alignment. With this factor, the relative permeability then becomes:[105]

$$S = \frac{1}{2}\left(3\cos^2\theta - 1\right) \tag{2.8}$$

$$\frac{P}{P_0} = \frac{1 - \Phi}{1 + \frac{1}{3}\alpha\Phi\left(S + \frac{1}{2}\right)} \tag{2.9}$$

Note that for perpendicular orientations, the relative permeability defaults to the Nielsen value.[105] In the Nielsen and Cussler models, filler particles were considered to be infinitely long ribbons in a polymer composite. Fredrickson and Bicerano were

the first to consider the filler particles as disks, which is more realistic. In order to do this, a convergent infinite series is derived, for which the first two terms sufficiently approximate the desired behavior:[106]

$$\frac{P}{P_0} = \frac{1}{4}\left(\frac{1}{1+\frac{2-\sqrt{2}}{4}\frac{\alpha\Phi}{\pi\ln\alpha}} + \frac{1}{1+\frac{2+\sqrt{2}}{4}\frac{\alpha\Phi}{\pi\ln\alpha}}\right)^2 \tag{2.10}$$

Finally, Gusev and Lusti contributed computational models of polymer composite barrier films. Monte Carlo simulations of a randomly-placed perpendicularly-aligned array of impermeable platelets, which is in close agreement with the models previously discussed:

$$\frac{P}{P_0} = \exp\left(-\left(\frac{\alpha\Phi}{3.47}\right)^{\beta}\right) \tag{2.11}$$

2.3 Graphene Oxide

Graphite oxide (graphene oxide, GO, is single sheets of graphite oxide) was first created in 1859 by Brodie.[108] He prepared pale yellow crystals of this material by repeated oxidation of Ceylon graphite in fuming nitric acid and potassium chlorate:

$$\text{graphite} \xrightarrow[5\,\text{x}]{\text{HNO}_3 + \text{KClO}_3} \text{GO} \tag{2.12}$$

He noted that the isolated product had an empirical formula of $C_{11}H_4O_5$ and that it "belongs very distinctly to the class of acids," which was ascertained from its solubility in basic solutions, but not in solutions containing acids or salts. Brodie also noted that the original graphitic appearance of the material could be restored if it was treated with reducing agents.

In 1870, Berthelot found that carbon from various sources, both amorphous

and graphitic, could be converted into the same kind of graphitic oxide found by Brodie.[109,110] In 1899, Staudenmaier treated Ceylon graphite with concentrated sulfuric and nitric acid, slowly adding potassium chlorate, yielding a green product. He then treated this with potassium permanganate and sulfuric acid, which together form the extremely oxidizing manganese heptoxide, to produce the yellow graphitic oxide:

$$\text{graphite} + H_2SO_4 \xrightarrow[2.\,KMnO_4]{1.\,HNO_3 + KClO_3} \text{GO} \tag{2.13}$$

This represented a significantly easier route than the multiple oxidations performed by Brodie and Berthelot.[111] Charpy studied the reaction conditions of previous syntheses in 1909 and found that mixing graphite with sulfuric acid in potassium permanganate yielded graphitic oxide at room temperature, but evolved carbon monoxide and dioxide in small quantities at 100 °C. Using chromic acid instead of permanganate, gas evolution increased substantially under similar conditions.[112] Balbiano determined that graphite oxide spontaneously exfoliates when heated rapidly. He also discovered that, while the color of the oxides is dependent on the absorption products of graphite, water, and carbon monoxide and dioxide, it is chemically similar.[113]

Building on these early studies, Hummers prepared graphite oxide by treating graphite with sodium nitrate and potassium permanganate in sulfuric acid:

$$\text{graphite} + H_2SO_4 + NaNO_3 + KMnO_4 \longrightarrow \text{GO} \tag{2.14}$$

The reaction mixture was so oxidizing that it needed to be kept in an ice bath initially to control the reaction rate. When compared with Staudenmaier's method, Hummers' method yields a much higher carbon-to-oxygen (C:O) ratio (2.25 vs. 2.89)

indicative of greater oxidation of the graphite. The method proposed by Hummers was so successful, it is the most common method currently available for producing graphene oxide.[114] In 1999, Kovtyukhova proposed that Hummers' method resulted in incompletely oxidized core-shell graphite/GO particles in the final product. To prevent this, a pre-oxidation step involving treatment of graphite powder with sulfuric acid, potassium peroxydisulfate, and phosphorus pentoxide (before performing Hummers' method, producing a much lower C:O ratio of 1.3) was utilized:[115]

$$\text{graphite} + H_2SO_4 \xrightarrow[2.\ NaNO_3 + KMnO_4]{1.\ K_2S_2O_8 + P_2O_5} \text{GO} \tag{2.15}$$

The newest method widely used to create GO was developed by Tour in 2010. In order to more completely oxidize graphite in a one step reaction, phosphoric acid was used in place of sodium nitrate:[116]

$$\text{graphite} + H_2SO_4 + KMnO_4 + H_3PO_4 \longrightarrow \text{GO} \tag{2.16}$$

The phosphoric acid has a critical role in the production of graphene oxide, as it is believed to form a five-membered cyclic phosphate group between it and two vicinal diols from the graphite basal plane, formed from oxidation with potassium permanganate. Using XPS, it was determined that Tour's method results in a greater sp^3 and lower sp^2 C1s signal than Hummers' method, which is indicative of a better oxidation.

The exact chemical structure of graphene oxide varies based on the type of graphite it originated from and the method used to produce it, but several attempts have been made to elucidate its chemical nature.[117,118] The earliest attempts from Hofmann determined that epoxide functionality was present and that the compound

should have an approximate stoichiometry of C_2O.[119] Reuss proposed that the basal plane of graphitic oxides was a mixture of sp^2 and sp^3 hydbridization, and hydroxyl functionality (bonded to cyclohexyl rings) existed through careful analysis of acidity, layer spacing, and solvent swelling characteristics.[120] Scholz later confirmed the presence of hydroxyl, carboxyl, and carbonyl functional groups (in quinone rings) and rejected the presence of ethers based on FTIR measurements.[121] These proposed structures are shown in Figure 2.13.

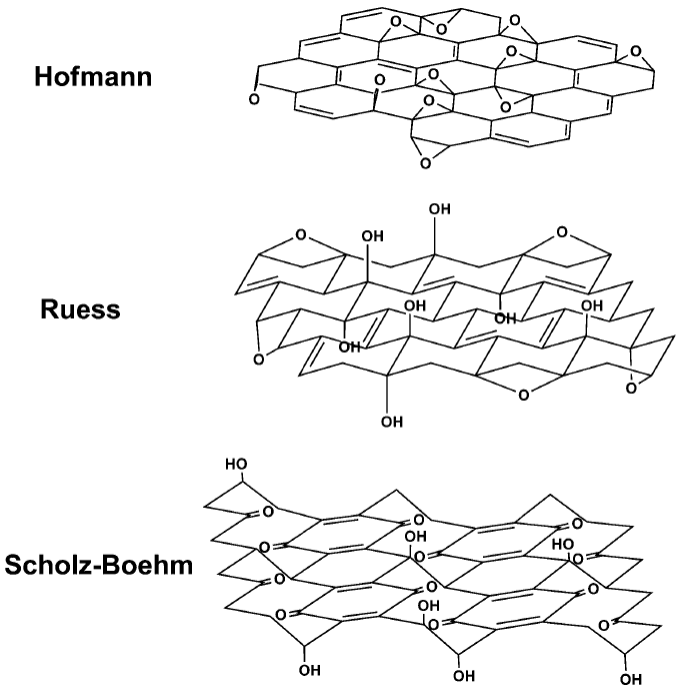

Figure 2.13: Proposed graphene oxide structures. Adapted from ref. [117].

Recent studies utilizing solid state nuclear magnetic resonance and reactivity to various reagents have produced greater structural detail of GO. Lerf and coworkers have been able to determine that GO contains hydroxyl, alkene, and at least two

inequivalent alcohols.[122,123] They also found that GO could be deoxygenated by HI and KI, reducing the presence of the ether signal, indicating that the ether signal was due solely to the presence of epoxide ethers rather than ethers formed in the basal plane. Reactivity towards hexamethylene diisocyanate causes cross-linking between platelets, confirming the presence of alcohols. Maleic anhydride, which acts as a dienophile for [4 + 2] cycloaddition, is largely unreactive, a result of highly conjugated or aromatic C-C double bonds.[124] This led to the modern structure of GO shown in Figure 2.14.[125]

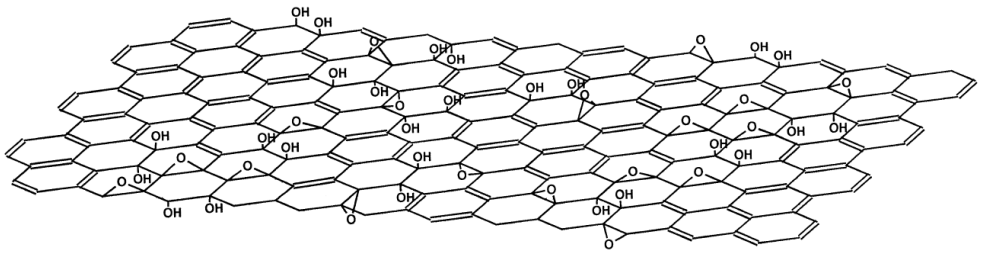

Figure 2.14: Modern approximate structure of GO, containing large amounts of hydroxyl and epoxy functional groups. Not shown are the carboxyl groups that are believed to form on the edges of the basal planes. Adapted from ref. [125].

The primary interest in graphene oxide stems from the fact that its oxygen-containing functional groups allow it to form stable suspensions in water, and that it can be reduced to a form similar to its graphite precursor, often called reduced graphene oxide (rGO).[117,126] Consequently, it has broad usage in fields such as field effect transistors,[127,128] transparent conductive thin films,[129,130] and fillers in polymer nanocomposites.[131,132] The reduction of graphene oxide is easily performed with heat,[11] UV light,[133,134] and various reagents including hydrazine,[135] ascorbic acid,[136] and hydriodic acid.[137] This reduction is obervable through FTIR (loss of epoxide

signal), Raman (**d** or disorder band decreases relative to the **g** or graphitic band), electrical conductivity (higher conductivity is observed with greater reduction), appearance (color changes from dark brown to reflective gray, similar to graphite), and XPS (the C1s intensity increases at 284.5 eV and decreases at 286.5, as shown in Figure 2.15).[11,117,137,138]

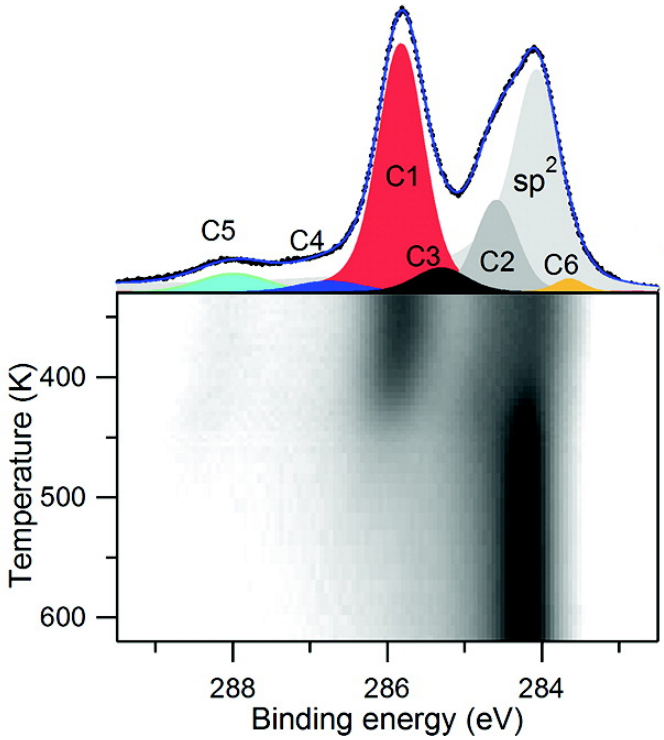

Figure 2.15: Evolution of C1s XPS spectrum of GO upon thermal reduction into rGO. The peak at 286.5 eV (which signals sp^3 C) decreases relative to 284.5 eV (which is present in pristine graphite due to its sp^2 character). Adapted from ref. [11].

III. HYDROPHOBICALLY-MODIFIED POLYELECTROLYTE FOR IMPROVED OXYGEN BARRIER IN NANOBRICK WALL MULTILAYER THIN FILMS *

3.1 Introduction

Polymer/clay thin film composites are of practical interest for their potential in reducing gas transmission. There has been a great deal of study in the area of thin film oxygen barriers,[92,140] though only recently have flexible, transparent, high gas barrier clay-filled composite films been reported.[74,141] SiO_x thin films are a much more mature technology, but propensity toward cracking when bent reduces their efficacy.[6] Polymer/clay bulk composites exhibit much higher oxygen permeability, and their poor transparency makes them less suitable for many packaging applications.[92] Layer-by-layer deposition of polyelectrolyte and clay nanoplatelets can produce thin films ($<$ 100 nm thick) with oxygen permeability up to two orders of magnitude less than SiO_x, with excellent transparency.[76]

In this study, pyrene was used to modify cationic polyethyleneimine (PEI) to impart greater hydrophobicity to quadlayer assemblies of PEI/poly(acrylic acid) (PAA)/PEI/clay. Side group functionalization of polyelectrolytes for layer-by-layer deposition has been previously reported for various purposes.[142,143] Pyrene was chosen because it is known to induce hydrophobic interactions as a side group for water-soluble polymers without causing water insolubility.[142,144–146] Labeling PEI with pyrene creates a more coiled polymer conformation, increasing the thickness and the associated clay spacing, which has been shown to decrease oxygen transmission

*Reprinted with permission from "Hydrophobically Modified Polyelectrolyte for Improved Oxygen Barrier in Nanobrick Wall Multilayer Thin Films" by Stevens, B. E. et al. *J. Polym. Sci., Part B: Polym. Phys.* **2014**, *52*, 1153–1156. ©2014 by Wiley-Blackwell.

rate (OTR) in these nanobrick wall assemblies.[32,74] Pyrene-labeled PEI (PEI-Py)-based multilayer nanocomposite films are 60 nm thick at three quadlayers, compared to 50 nm for the same system prepared with unmodified PEI-based films. For only twelve deposited layers, OTR of PEI-Py-based films is more than 10x better than the PEI-based film. Covalent modification of polyelectrolytes for layer-by-layer assembly provides a new route for reducing the number of deposition steps required to achieve high gas barrier, making this technology much more feasible for use in various packaging applications (food, electronics, etc.).

3.2 Experimental

3.2.1 Materials

Polyethyleneimine (PEI) (M_w = 25000 g/mol, PDI = 2.5), poly(acrylic acid) (PAA) (M_w = 100000 g/mol), 1-pyrenecarboxaldehyde (Py-CA), sodium borohydride ($NaBH_4$), dichloromethane, and methanol were obtained from Sigma-Aldrich (St. Louis, MO). Sodium montmorillonite (MMT) was obtained from Southern Clay Products (Gonzalez, TX). Individual MMT platelets have a reported density of 2.86 g/cm^3, diameter of 10–1000 nm, and thickness of 1 nm.[147] All chemicals were used as received. Poly(ethylene terephthalate) (PET) film with a thickness of 179 µm was purchased from Tekra (New Berlin, WI) and used as the substrate for OTR testing. Single side polished (100) silicon wafers (University Wafer, South Boston, MA) were used as substrates for film thickness characterization. Polished Ti/Au quartz crystals were used for quartz crystal microbalance (QCM, Maxtek, Inc., Cypress, CA) measurements.

Pyrene-labeled PEI was prepared using a modification of a previously reported reductive amination method,[146] summarized in Figure 3.1. Ten grams of PEI was mixed with 15 mL of 18M deionized water and 80 mL of methanol. The pH of this

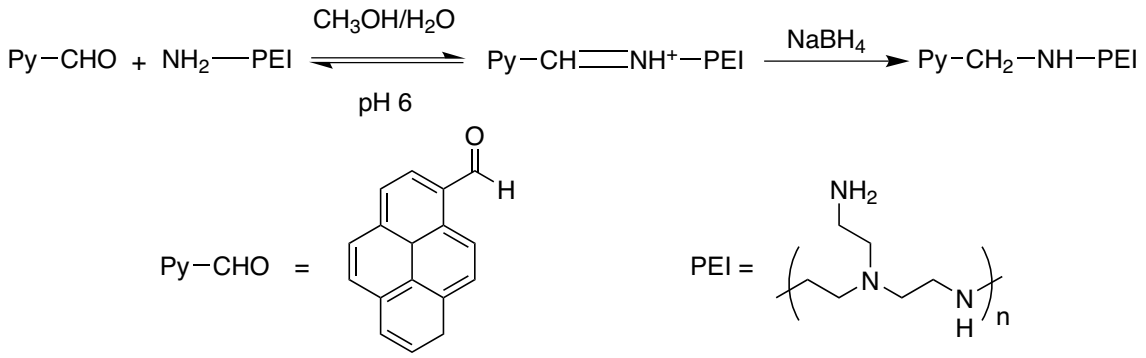

Figure 3.1: Synthetic procedure for pyrene-labeled polyethyleneimine.

solution was adjusted to 6 using 1M HCl. 500 mg of Py-CA was added and stirred to form a hazy, light yellow mixture. Excess $NaBH_4$ (410 mg was added to the solution and allowed to react for 20 h to yield a translucent, pale yellow solution. The solution was dried by rotary evaporation, producing a viscous yellow liquid, which was dissolved in 50 mL H_2O and washed three times with dichloromethane. The aqueous phase was collected and dried to remove any remaining dichloromethane, yielding approximately 10 g of viscous yellow liquid.

3.2.2 Polymer Characterization

Fourier transform infrared spectra were obtained by a Bruker Optics Inc. ALPHA FT-IR spectrometer with a universal sampling module operating in transmittance mode. Samples were dried on ZnSe at 110 °C for 1 h prior to measurement. PEI and PEI-Py samples were cast from aqueous solutions, whereas Py-CA was cast from a solution of dichloromethane.

3.2.3 Film Deposition

Each deposition solution was prepared using deionized water and rolled for 24 hours before use. The pH of 0.1 wt% PEI solutions was altered to 10 using 1M

HCl, while 0.1 wt% PEI-Py was altered to pH 10 using 1M NaOH. The pH of 0.2 wt% PAA solutions was altered to 4 using 1M NaOH. Aqueous suspensions of anionic MMT (1.0 wt. %) were unaltered, having a pH of 9.9. PET substrates were prepared for deposition by rinsing with deionized water, methanol, and water again before being dried with filtered air. The film was then corona treated to induce a strong negative surface charge,[148] using a BD20C Corona Treater (Electro Technic Products, Inc., Chicago, IL). Silicon wafers and QCM crystals were treated with oxygen plasma in preparation for deposition.[149] Each appropriately treated substrate was dipped in a PEI or PEI-Py solution for 5 min., rinsed with deionized water, and dried. This procedure was followed by an identical dipping, rinsing and drying procedure in the PAA solution. After this initial bilayer was deposited, the same procedure was followed with one minute dip times for subsequent layers in a pattern of PEI/PAA/PEI/MMT or PEI-Py/PAA/PEI-Py/MMT. This procedure was repeated until the desired number of quadlayers was achieved. All thin films were prepared using homebuilt robotic dipping systems.[149] Films created for OTR testing were heated in an oven for 15 min at 70 °C immediately following deposition.

3.2.4 Film Characterization

Thickness of polymer/clay assemblies, coated on silicon wafer, was measured with a KLA-Tencor (Milpitas, CA) P6 profilometer. Deposited mass was measured by QCM (Maxtek). Oxygen transmission rate (OTR) testing was performed by MOCON (Minneapolis, MN), at 0% RH and 23 °C using an Oxtran 2/21 instrument, in accordance with ASTM D3985.

3.3 Results and Discussion

FT-IR spectra for 1-pyrenecarboxaldehyde (Py-CA), polyethyleneimine (PEI), and pyrene-labeled PEI (PEI-Py) are shown in Figure 3.2. The PEI-Py spectrum

shows the presence of weak aromatic overtone peaks in the 1700-2000 cm^{-1} range and two C-H stretching frequencies at 2870 cm^{-1} and 2970 cm^{-1} (also present in the 1-pyrenecarboxaldehyde (Py-CA) spectrum). The broad N-H absorption from the PEI is also observed in the spectrum for PEI-Py. Notably absent in the PEI-Py spectrum are the C=O (1700 cm^{-1}) and aldehyde C-H (3050 cm^{-1}) bands that are present in the Py-CA spectrum, confirming reduction of the aldehyde.

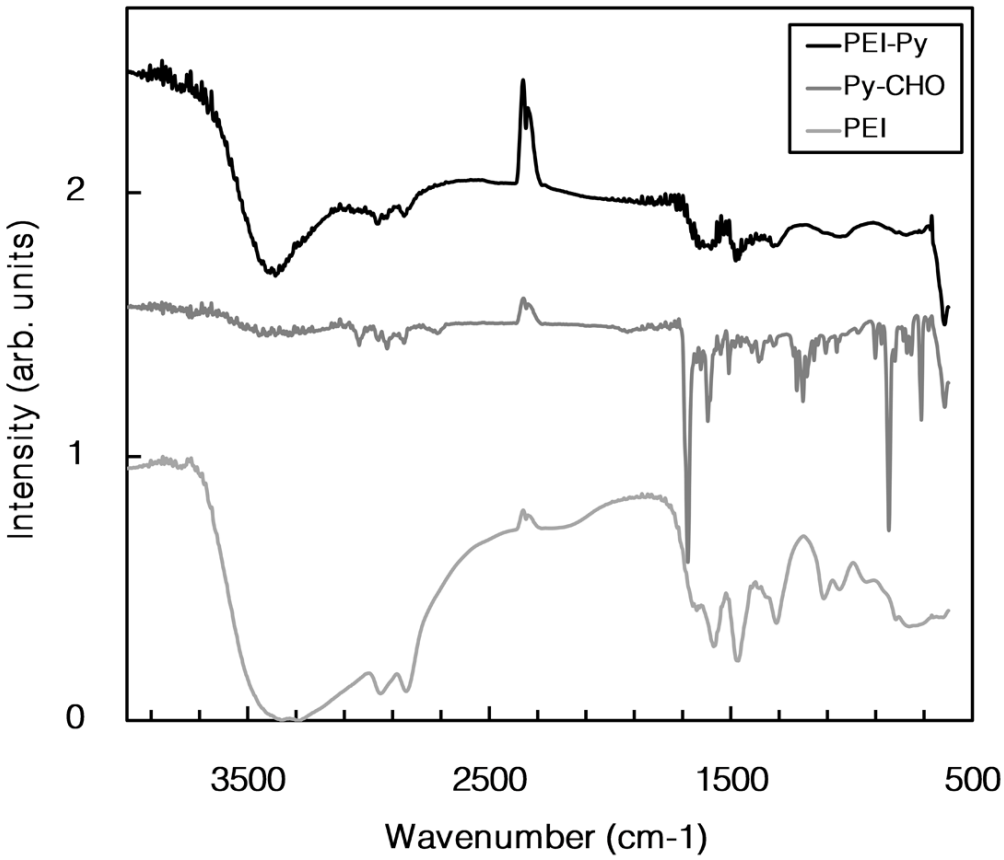

Figure 3.2: FT-IR spectra of neat PEI, Py-CA, and PEI-Py.

During layer-by-layer deposition, the initial primer layer adheres to the substrate by electrostatic attraction to the negatively charged surface created by either corona treatment (for poly(ethylene terephthalate) (PET)) or plasma treatment (for silicon). Each subsequent layer is created by dipping the substrate in a solution containing material of the opposite charge of the layer deposited just prior. By alternately dipping the substrate into oppositely charged solutions, the surface charge on the substrate switches between positive and negative, and the film thickness increases through these attractions. Figure 3.3 shows the exponential growth of these quad-layer recipes, as measured by profilometry, which is expected when using multiple weak polyelectrolytes.[76,150] The seemingly exponential growth of these films is attributable to the interdiffusion of PEI (or PEI-Py) and PAA.[151,152]

The presence of pyrene groups on the polymer has previously been shown to result in hydrophobic interactions for water-soluble poly(ethylene glycol),[144] which results in a shift in conformation from extended to coiled. This coiled conformation results in both thicker and denser deposition of PEI-Py onto the previous layer compared to unmodified PEI. Weight of films (from quartz crystal microbalance (QCM)) was divided by thickness and quartz crystal area to determine film densities shown in Table 3.1, which confirms greater density of PEI-Py assemblies. Increasing pH could produce thicker PEI growth, but significant differences between pH of cationic and anionic solutions can cause destabilization and detachment of these assemblies.[30,153,154] Altering the polymer conformation and introducing hydrophobic groups, rather than simply adjusting pH, circumvents problems associated with destabilization, and higher density PEI layers are formed that improve gas barrier.

Cussler and coworkers predicted that films composed of layers of impermeable flakes would have greatly decreased gas diffusion,[102] which was experimentally confirmed in previous studies of platelet-based assemblies.[32,76,141,155,156] Table 3.1 shows

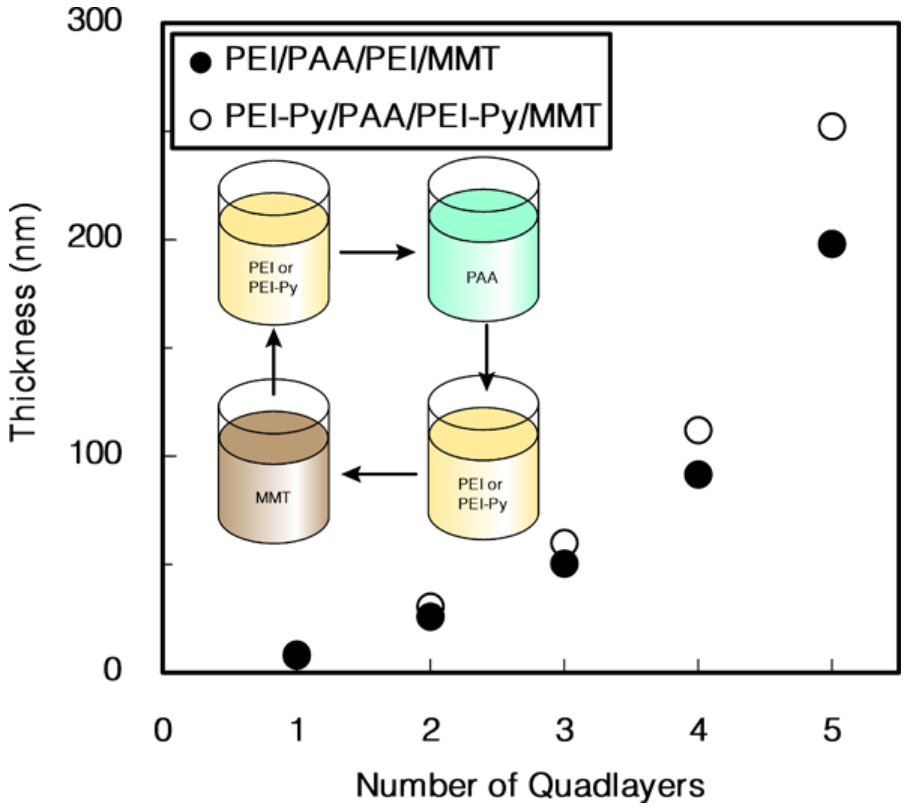

Figure 3.3: Thickness of PEI and PEI-Py films as a function of quadlayers deposited. The inset shows the LbL deposition sequence.

OTR values for PEI and PEI-Py based films on PET. The OTR decreases with increasing film thickness, but film density plays an important role as well. Although 3 quadlayers (QL) PEI-Py films are only 10 nm thicker than 3 QL PEI films, higher density of PEI-Py led to an order of magnitude reduction in OTR and permeability of the coating.

The synthesis of pyrene-labeled polyethylenimine, and its use in multilayer nanocomposite thin films, was evaluated as a means of increasing density and spacing between clay layers (without altering pH). Layer-by-layer deposition of PEI (or PEI-Py), PEI, and clay platelets resulted in similar thickness, but significantly higher density for

Table 3.1: Film thickness and oxygen transmission rate for quadlayers deposited on PET.

System	Film Thickness (nm)	Film Density $\left(\frac{\text{g}}{\text{cm}^3}\right)$	OTR $\left(\frac{\text{cm}^3}{\text{m}^2 \cdot \text{day} \cdot \text{atm}}\right)$	Coating Permeability $\left(10^{-21}\,\frac{\text{cm}^2}{\text{Pa} \cdot \text{s}}\right)$	Total Permeability $\left(10^{-18}\,\frac{\text{cm}^2}{\text{Pa} \cdot \text{s}}\right)$
Bare PET	0	N/A	8.6	N/A	1750
3 PEI QL	50	1.24	0.75	94	150
4 PEI QL	92	1.24	0.045	9.4	9.1
3 PEI-Py QL	60	1.45	0.059	8.1	12
4 PEI-Py QL	112	1.70	0.028	7.2	5.7

films made with PEI-Py, rather than PEI, due to hydrophobic interactions that cause the polymer to adopt a more coiled conformation. Three PEI-Py-based quadlayers deposited on PET exhibited an oxygen transmission rate similar to four PEI-based QL as the result of greater layer density. It is believed that this approach could be applied more universally to grow denser layer-by-layer films able to achieve higher barrier with fewer layers.

IV. LOW TEMPERATURE THERMAL REDUCTION OF GRAPHENE OXIDE NANOBRICK WALLS: UNIQUE COMBINATION OF HIGH GAS BARRIER AND LOW RESISTIVITY IN FULLY ORGANIC POLYELECTROLYTE MULTILAYER THIN FILMS *

4.1 Introduction

Strong interest in traditional (and flexible) organic electronics is driving the need for electrically conductive layers with high oxygen barrier properties that can be applied using low cost methods.[1,157] Commercially available options for surface coatings that meet these requirements rely on expensive vapor phase application under vacuum,[4] such as SiO_x, Al_xO_y, and metallized films, which are subject to cracking and pinhole defects.[6,8] While graphene, a single layer flake of sp^2 carbon atoms, can be difficult to work with due to high van der Waals interactions,[158] graphene oxide (GO) is amenable to aqueous processing due to its abundance of hydrophilic functional groups.[117] While both graphene and GO have been found suitable for their impermeability to a variety of gases,[34,159] the latter is an electrical insulator. Electrical conductivity can be enhanced by chemical or thermal reduction to form reduced graphene oxide (rGO), which often displays properties necessary for flexible electronics.[160,161] The multipurpose nature of graphene oxide, combined with the straightforward layer-by-layer (LbL) process, creates an opportunity for inexpensive application for electronics packaging and other types of encapsulation.

Graphene oxide has been shown to display gas barrier[34] and electrical conductivity,[35,162] when applied using layer-by-layer processing, but the barrier properties

*Reprinted with permission from "Low-Temperature Thermal Reduction of Graphene Oxide Nanobrick Walls: Unique Combination of High Gas Barrier and Low Resistivity in Fully Organic Polyelectrolyte Multilayer Thin Films" by Stevens, B. et al. *ACS Appl. Mater. Interfaces* **2014**, *6*, 9942–9945.

were not retained under humid conditions and electrical conductivity required exposure to toxic chemicals (e.g., hydrazine). When heated to 175 °C in air for 90 minutes, graphene oxide undergoes reduction and, in a multilayer assembly with polyethyleneimine, displays both low sheet resistance (< 5 kΩ/□) and oxygen permeability (e.g., the oxygen transmission rate is 3-4 orders of magnitude lower than uncoated poly(ethylene terephthalate)) under dry as well as humid conditions. The extent of GO reduction, and hence electrical resistance and gas permeability, may be tuned by varying the temperature and exposure time.

4.2 Experimental

4.2.1 General Materials and Methods

All reagents were used as received from Sigma-Aldrich (St. Louis, MO) unless otherwise noted. Solutions of polyethyleneimine (PEI) (M_n = 10000 g/mol and M_w = 25000 g/mol) were prepared by dissolving PEI in 18.2 MΩ deionized water (DI H_2O) and rolling the solution in a bottle overnight before adjusting pH using 1 M HCl. Suspensions of graphene oxide (GO) (see next section for more information) were prepared by crushing GO powder with DI H_2O in a mortar and pestle to form a paste, which was then added to the correct amount of DI H_2O required to reach the desired concentration and sonicated using a Misonix XL 2000 ultrasonic cell disruptor (Misonix Inc., Farmingdale, NY) at 15 W for 10 min. GO suspensions were used for layer-by-layer assembly directly after sonication. Single-side polished (100) silicon wafers (University Wafer, South Boston, MA) were piranha treated with a 3:1 mixture of concentrated sulfuric acid to 30% hydrogen peroxide. Caution: piranha solution reacts violently with organic material and proper safety and handling precautions should be taken. Prior to use, silicon wafers were rinsed with acetone and DI H_2O. Poly(ethylene terephthalate) (PET) film with a thickness of 175 µm (trade

name ST505 from Dupont-Teijin) was used as a substrate for four point probe measurement, oxygen transmission rate measurement, and electron microscopy. PET was rinsed with DI water and methanol prior to use. PET substrates were then corona treated with a BD-20C corona treater (Electro-Technic Products Inc., Chicago, IL).

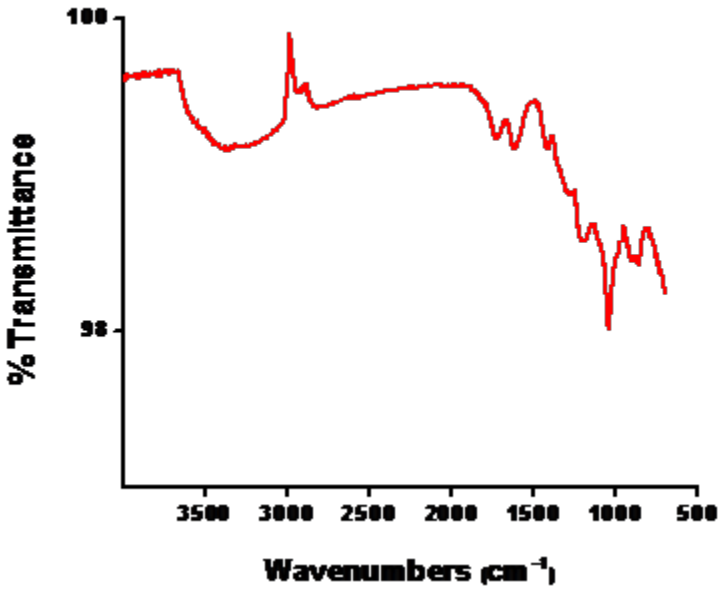

Figure 4.1: FT-IR spectra of as-prepared GO.

4.2.2 Preparation of Graphite Oxide (GO)

A 250 mL round-bottom flask was charged with a stir bar, natural flake graphite (6.04 g, Bay Carbon SP-1), concentrated H_2SO_4 (150 mL), and then cooled in an ice bath. The flask was slowly charged with $KMnO_4$ (18.13 g, 114.74 mmol) over 2 hours which produced a dark colored mixture. After stirring at 0 °C for an additional 1 hour, the mixture was then stirred at room temperature for 2 hours and finally at

35 °C for 3 hours. After cooling to room temperature, the mixture was added to deionized water (3 L) which resulted in an exotherm. To the resulting suspension was added a 30% aqueous solution of H_2O_2 (15 mL), and the vibrant yellow suspension was allowed to sit overnight. The GO was isolated by centrifugation and subsequent decantation of the supernatant after being washed with 6 N HCl (3 L) and deionized water (6 L) respectively. The precipitate was collected and dried under high vacuum to afford the product (11.15 g) as a dark brown powder which was characterized by elemental combustion, FT-IR spectroscopy, and BET analysis.

4.2.3 GO Characterization

IR spectra were recorded on a Thermo Scientific Nicolet iS5 system equipped with an iD3 attenuated total reflectance (ATR) attachment (germanium crystal). BET surface area analyses were determined using nitrogen adsorption on a Quantachrome NOVA 2000 surface analyzer. Elemental combustion analyses were determined by Midwest Microlabs, LLC (Indianaopolis, IN).

Table 4.1: Elemental abundance in GO and thermally-reduced GO.

Element	Starting GO Material	Thermally-Reduced GO
Carbon	51.02	80.1
Hydrogen	1.65	1.06
Nitrogen	none found	none found
Oxygen	44.50	17.52
Sulfur	1.85	1.11
Chlorine	0.92	not determined

4.2.4 BET Measurements

The samples were degassed at room temperature to avoid thermal decomposition of GO, and measurements were determined using a 7-point BET method using molecular nitrogen as the adsorbate.[163] Measurements were performed in triplicates and the values were averaged.

Table 4.2: BET Surface Area Analysis of GO and thermally-reduced GO

Carbon Material	Surface Area m^2/g
GO	2.5
Thermally-Reduced GO	855.4

4.2.5 Layer-by-Layer Assembly Procedure

The layer-by-layer process is illustrated in Figure **??** (a). In a typical procedure, a given substrate was immersed in PEI solution for 5 min, followed by a rinse with DI water and drying with filtered air to form the first positively-charged layer. The substrate was then immersed in GO solution for another 5 min, followed by another rinse and dry sequence. Single-minute dips in PEI and GO solutions, followed by rinse and dry sequences, were then repeated for the desired number of cycles. This process was carried out using a home-built robotic dipping system controlled by LabView (National Instruments, Austin, TX).[141,149]

4.2.6 Thin Film Characterization

Thickness of PEI/GO LbL assemblies, coated on silicon wafer, was measured with a KLA-Tencor P6 profilometer. Sheet resistance was measured using a four point

probe apparatus (Signatone Corporation, Gilroy, CA) controlled with home built LabView program. Oxygen barrier testing was performed by Mocon, Inc. on an Ox Tran 2/21 L module at 23 °C in both 0% and 100% relative humidity conditions on both sides of the coated substrate. Scanning electron micrographs were taken using a JEOL JSM-7500F in Gentle Beam mode to reduce charging of the films. Samples for transmission electron microscopy (TEM) were prepared by embedding coated PET films in epoxy and sectioning them with a microtome. TEM micrographs were obtained by imaging these sections with an FEI Tecnai G2 F20 FE-TEM.

4.3 Results and Discussion

Synthesis of graphene oxide proceeded as previously reported.[114] The FT-IR spectrum of the freshly-prepared GO is shown in Figure 4.1. The FT-IR spectrum indicates the presence of the expected carboxylic acid, alcohol, and epoxide functionalities. Elemental analysis of GO and thermally-reduced GO showed a marked decrease in oxygen relative to carbon upon heating (Table 4.1). Though similar in chemical nature, BET measurements of the starting graphite and thermally-reduced graphene oxide reveal that the oxidation and subsequent reduction leaves the thermally reduced graphene oxide well-exfoliated compared to graphite powder (Table 4.2).

Thin film growth was achieved with an aqueous PEI solution (0.1 wt% at pH 10) and aqueous graphene oxide (GO) suspension (0.1 wt% at pH 3.3) through an alternating deposition sequence on PET film. As illustrated in Figure **??** (a), this layer-by-layer process resulted in anion-cation bilayers on the substrate through the formation of electrostatic interactions. Profilometry was used to monitor the thickness of these films, both as-prepared and after thermally reducing the films at 175 °C for 90 minutes, as shown in Figure **??** (b).

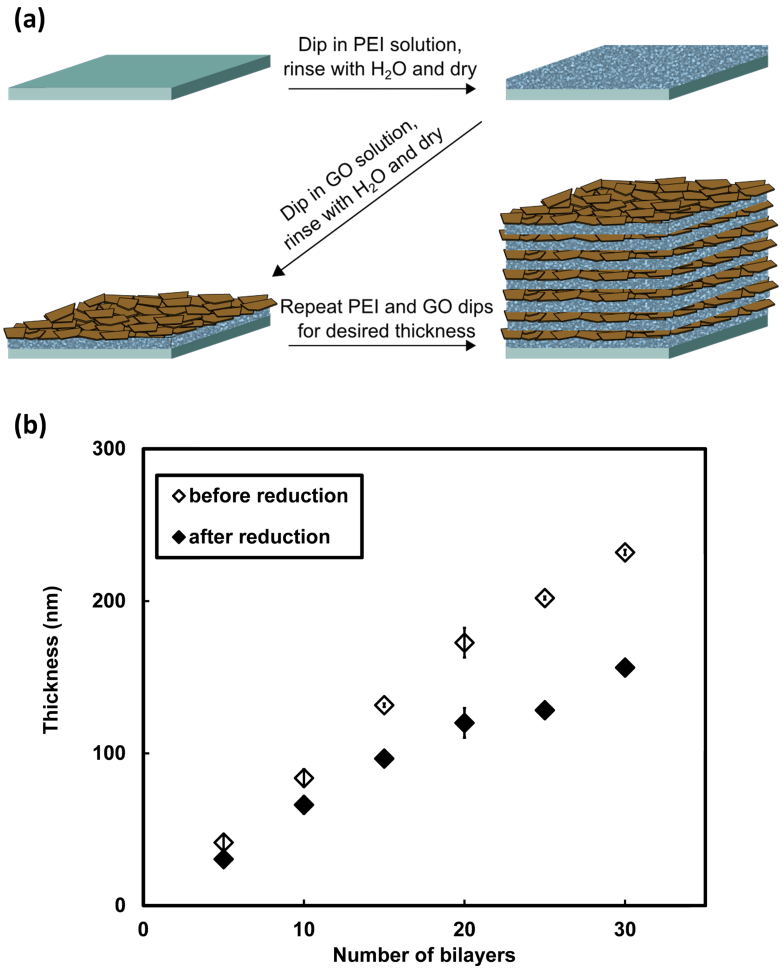

Figure 4.2: Schematic of layer-by-layer deposition of polyethyleneimine and graphene oxide bilayers onto a substrate (a) and profilometer thickness of PEI/GO assemblies grown on silicon before and after reduction at 175 °C for 90 minutes (b).

At 20 bilayers, the film thickness was approximately 173 nm, as measured on silicon, although thermal reduction reduces this value to 120 nm (i.e., 70% of original thickness). Additionally, the coverage of GO was uniform across the assembly, and the observed wrinkling of GO platelets diminished upon reduction (Figure 4.3 (a,b)). The TEM images indicated that GO platelets were aligned parallel to the direction of the substrate and packed closely together (Figure 4.3 (c)). Although the density

of graphene oxide appearred to be high, the film was optically transparent until it was thermally reduced (Figure 4.3 (d)), at which point the film obtains a metallic luster similar to that of graphite.

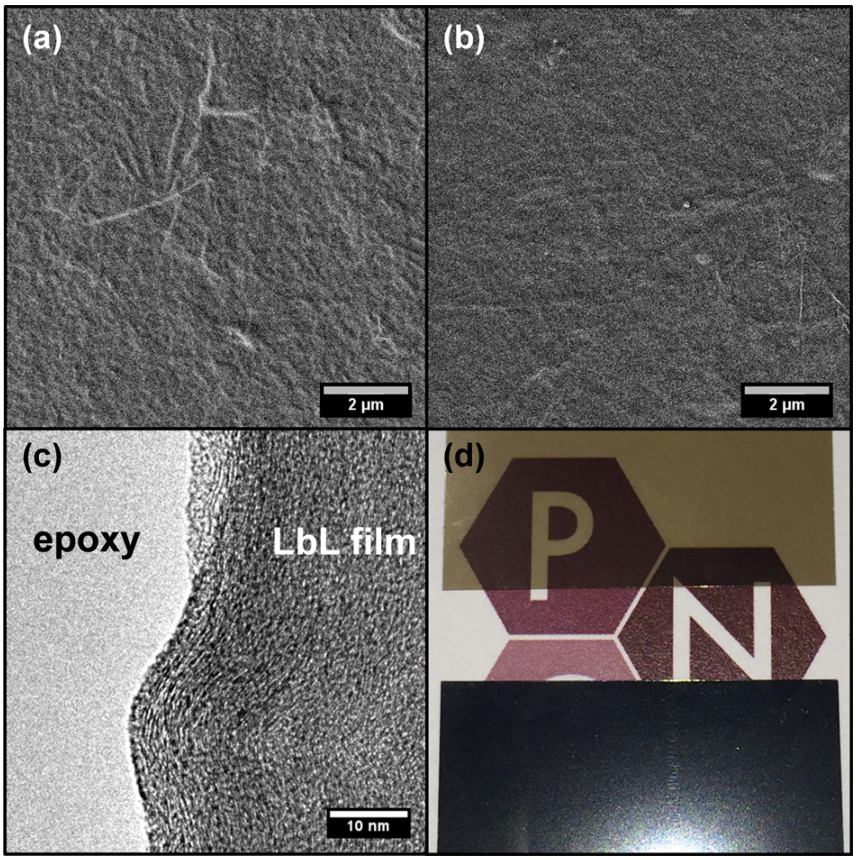

Figure 4.3: SEM micrographs of 20 bilayer PEI/GO assemblies before (a) and after (b) 90 minute thermal reduction at 175 °C. TEM micrograph of the same thin film before reduction (c), showing GO oriented parallel to the film. Thermal reduction of a 10-bilayer assembly results in the originally transparent film (d, top) becoming opaque, with a graphitic luster (d, bottom).

Thermal reduction of GO was monitored by electrical conductivity and X-ray photoelectron spectroscopy (XPS) measurements. In the most reduced state, the

PEI/GO films exhibited a decrease in electrical sheet resistance by more than four orders of magnitude. Four-point probe resistivity measurements indicated that electrical sheet resistance decreased from $> 10^7$ $\Omega/\square$ to 4760 $\Omega/\square$ following a 90-minute reduction at 175 °C (in an ambient atmosphere), corresponding to a conductivity of 1750 S/m. Increased electrical conductivity was the result of partial restoration of sp^2 carbon bonds in the reduced GO. XPS revealed a decrease in C1s peak intensity at 286.5 eV, relative to 284.5 eV (Figure 4.4), indicative of fewer C-O bonds and higher sp^2 carbon content characteristic of graphite.[11]

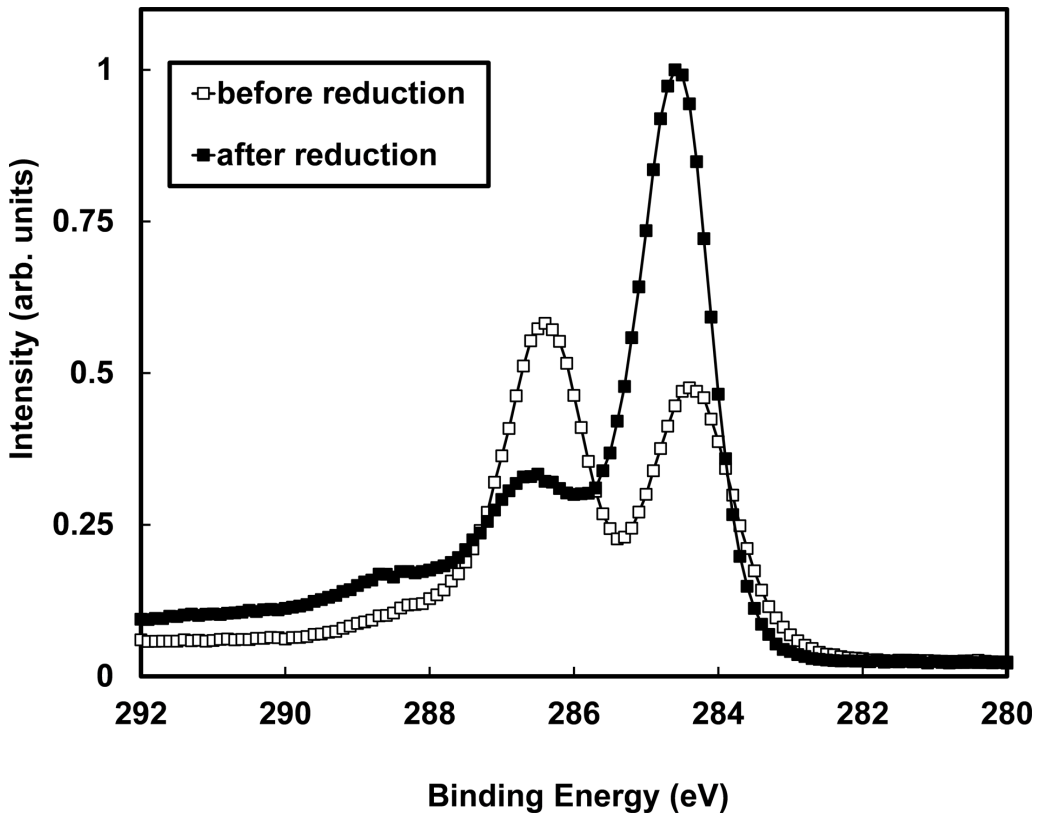

Figure 4.4: C1s XPS spectrum of graphene oxide before and after a 90-minute reduction at 175 °C. Increase in peak intensity at 284.5 eV, relative to 286.5 eV, after reduction reflects partial restoration of graphitic character of GO.

It is important to note that the reduction conditions used for these PEI/GO assemblies on 175 µm thick, commercial-grade PET were mild, and no loss of film or substrate integrity was observed by SEM. Because these assemblies displayed a continuum of electrical resistivities between their pre-reduced and maximally reduced states (Figure 4.5), it is apparent that the degree of reduction may be tailored, along with the associated properties.

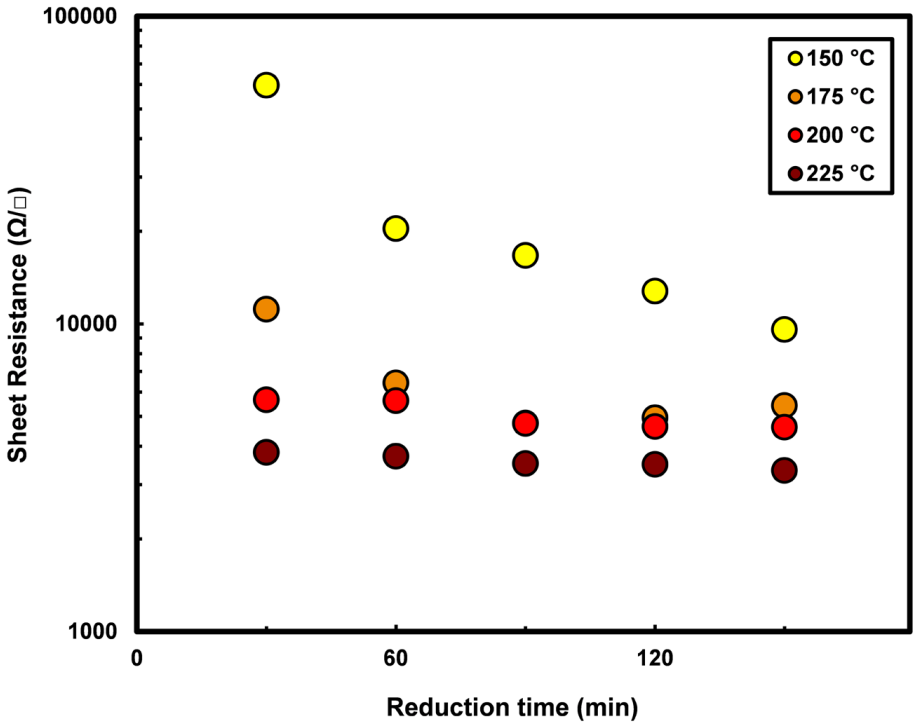

Figure 4.5: Sheet resistance as a function of exposure time, for 20 bilayer PEI/GO assemblies, to various thermal reduction temperatures (see legend). The standard deviation for the five measurements taken for each data point is smaller than the size of the markers for the points.

The oxygen barrier properties of these assemblies were measured with oxygen

transmission rate (OTR) testing of coated PET samples, in both 0% (dry) and 100% (humid) relative humidity conditions. The results of this testing are summarized in Table 4.3. Prior to thermal reduction, the GO/PEI multilayer thin films displayed excellent barrier properties to oxygen under dry conditions; indeed, with as few as 10 bilayers, dry OTR decreased from 8.6 to 0.0078 $cm^3/m^2/d/atm$. Depositing 20 PEI/GO bilayers caused the OTR to drop below the detection limit of the commercial instrumentation (< 0.005 $cm^3/m^2/d/atm$). When a 90-minute thermal reduction at 175 °C was applied to these 10 and 20 bilayer assemblies, both exhibited OTR values below detection. Reduction of the GO decreased 10 bilayer film permeability, from 14.9 to $< 7.03 \times 10^{-22}$ $cm^2/Pa/s$,[157] a value comparable to the lowest reported dry oxygen film permeability measured for an LbL film.[76]

Under humid conditions, pre-reduced and reduced assemblies show a wide disparity. With 20 bilayers deposited, the OTR of GO/PEI exhibited little improvement over bare PET, decreasing by less than a factor two. When thermally reduced, the humid OTR of the resulting rGO/PEI assemblies decreased to 0.98 and 0.022 $cm^3/m^2/d/atm$ for 10 and 20 bilayer films, respectively. Though dry OTR barrier was not fully retained, these assemblies reduced oxygen transmission substantially better than bare PET. GO-based assemblies have displayed a propensity for dry oxygen barrier applications,[34] but humid oxygen barrier has been difficult to achieve due to the hydrophilic nature of the assemblies that leads to swelling and increased permeability.[164,165] Compaction of PEI/GO assemblies upon reduction effectively increased the nanoplatelet concentration, and hydrophilic GO was transformed into hydrophobic rGO, inhibiting film swelling.

Table 4.3: Oxygen transmission rate and permeability data for GO/PEI assemblies on PET, before and after a 90-minute thermal reduction at 175 °C.

System		Film Thickness (nm)	Relative Humiditiy (%)	OTR $\left(\frac{\text{cm}^3}{\text{m}^2 \cdot \text{day} \cdot \text{atm}}\right)$	Total Permeability $\left(10^{-15}\,\frac{\text{cm}^2}{\text{Pa} \cdot \text{s}}\right)$	LbL Film Permeability $\left(10^{-18}\,\frac{\text{cm}^2}{\text{Pa} \cdot \text{s}}\right)$
Bare PET				8.6	1.7	
10 BL	unreduced	84	0	0.0078	0.0016	0.0015
	reduced	66	0	<0.0047	<0.00095	<0.00070
	unreduced	84	100	5.8	1.2	3.3
	reduced	66	100	0.98	0.20	0.17
20 BL	unreduced	173	0	<0.0047	<0.00095	<0.0018
	reduced	120	0	<0.0047	<0.00095	<0.0018
	unreduced	173	100	5.4	1.1	5.8
	reduced	120	100	0.022	0.0044	0.0060

Nanocoatings with high conductivity and low oxygen permeability are very desirable for electronics packaging applications.[1,157] Ambient processing from aqueous solutions provides a simple and cost-effective route to graphene oxide-based thin films with these properties. Relatively low temperature (< 200 °C) treatment in air affords the ability to improve electrical sheet resistance and film permeability. The increased hydrophobicity of the reduced thin film results in decreased permeability that is retained at high humidity. Collectively, the exceptional functionality and flexible nature of these coatings, along with the ease with which they are applied, makes them ideal for use in a variety of electronics packaging and encapsulation applications.

V. SOFT PATTERNING OF CONDUCTIVE GRAPHENE OXIDE-BASED MULTILAYER THIN FILMS

5.1 Introduction

Growing interest in flexible organic electronics is driving the need for electrically conductive layers that can be applied using low cost methods.[1] Patterned conductive surfaces are ubiquitous in electronic devices, being commonly utilized in printed circuit boards (PCBs) and integrated circuits (ICs). Traditional PCBs and ICs are designed around rigid substrates: epoxy for PCBs and silicon/silicon dioxide for ICs. Rigid substrates are unsuitable for flexible electronics, and the fabrication of these patterned surfaces is complicated, expensive, and potentially dangerous.[12] PCB patterning uses either electroplating or electroless plating, both of which produce a considerable amount of toxic side products and environmental pollutants.[13,14] IC fabrication, through commonly-used photolithography, results in a large number of contaminants from chemicals used to treat wafers.[15,16] Patterning of conductive pathways on flexible substrates is not currently done using these technologies, though both would benefit substantially from simplified environmentally-friendly techniques.

In this study, layer-by-layer (LbL) processing is used to deposit an electrically conductive thin film from aqueous solutions. The thickness and morphology of the deposited layers may be tuned by varying processing conditions (e.g. pH[29] and concentration[30]) of the requisite solutions, which ultimately influences the macroscopic properties.[31–33] Exposure of these films to sufficiently high or low pH environments causes degradation of many of these assemblies,[153,154] which can serve as a means to pattern them.[166] Charged nanoparticles are often incorporated into these films, such as clay and graphene oxide (GO).[29,32,33,35,99,139] When GO is used in LbL as-

sembly, electrical conductivity is attainable through a chemical or thermal reduction step.[35,99] LbL processing with GO and polyethyleneimine (PEI) has been shown to create coatings that are both impermeable to gas and electrically conductive.[139]

Patterning of circuits for electronics can be a much safer and less expensive process if durable electrically conductive pathways can be applied from aqueous solutions of benign materials and processed under ambient or near-ambient conditions using a wet etching technique based on wet stamping (WETS).[167,168] In this case, patterned agarose hydrogel stamps are soaked in a solution of interest and stamped onto the substrate, causing a reaction between the solution and substrate that can result in patterned features. This technique has been successfully demonstrated with LbL assemblies, achieving ∼10 µm resolution.[166] The WETS technique is used here to selectively etch graphene oxide-based LbL assemblies, which can then be reduced to form electrically conductive features. The exposure process, in which the PEI/GO film is exposed to mildly basic solutions (∼0.05 M NaOH) results in a patterned surface. Successful etching of the film results in complete detachment from the substrate, ensuring short circuiting in these conductive patterns will not occur. When compared with traditional lithographic methods, such as photolithography, this WETS approach significantly reduces the expense and danger involved in creating these patterns.

5.2 Experimental

5.2.1 Materials and Methods

All reagents were used as received from Sigma-Aldrich (St. Louis, MO) unless otherwise noted. Solutions of polyethyleneimine (PEI) (M_n = 10000 g/mol and M_w = 25000 g/mol) were prepared by dissolving PEI in 18.2 MΩ deionized water (DI H_2O) and rolling the solution in a bottle overnight before adjusting the pH to 10 using

1 M HCl. Suspensions of graphene oxide (GO, Cheap Tubes Inc., Cambridgeport, VT) were prepared by crushing GO powder in a mortar and pestle with water until a paste was obtained. This paste was then added to deionized water to form a 0.1 wt% suspension and sonicated using a Misonix XL 2000 ultrasonic cell disruptor (Misonix, Inc., Farmingdale, NY) at 15W for 10 min. The GO suspensions, which start with a pH of ∼3.2, were either used unaltered or were pH adjusted before use with 0.1 M HCl or 0.1 M NaOH to reach pH values of 2.75, 3, 3.25, 3.5, 3.75, 4, 6, 8, and 10. Agarose was obtained from Sigma-Aldrich and used as received. Single-side polished (100) silicon wafers (University Wafer, South Boston, MA) and glass microscope slides (Corning Inc., Corning, NY) were exposed to oxygen plasma for 10 min prior to use. Zeta potential of GO was measured using a Brookhaven Instruments ZetaPALS zeta potential analyzer (Long Island, NY). Fourier transform infrared spectra were obtained by a Bruker Optics Inc. ALPHA FT-IR spectrometer (Billerica, MA) with a diamond ATR unit.

5.2.2 Layer-by-Layer Assembly Processing

The layer-by-layer procedure is shown graphically in Figure 5.1(a). The silicon or glass substrate was immersed in PEI solution for 5 min., rinsed with DI water, and dried with filtered air. This substrate was then immersed in GO suspension for 5 min, followed by the same rinse and dry. The cycle of PEI dip, rinse and dry followed by GO dip, rinse and dry was continued with 1 minute immersions to produce the desired number of bilayers (BL). This process is carried out using a home-built robotic dipping system controlled by LabView (National Instruments, Austin, TX).[141] The resulting film has the approximate structure shown in Figure 5.1(b).

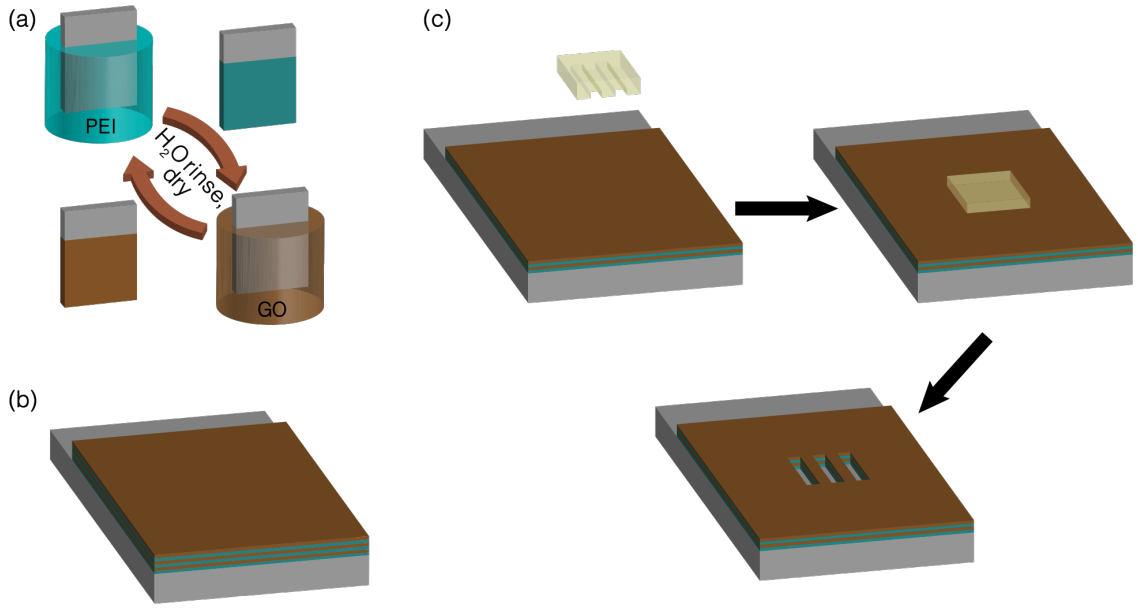

Figure 5.1: Schematic of the layer-by-layer (LbL) process, involving alternating immersions of a given substrate in aqueous solutions of PEI and GO, with a rinse and dry step in between (a). LbL assembly results in a multilayer coating of the two solution ingredients on a substrate surface (b). The coated substrate is then exposed to the wet stamping (WETS) process (c), in which an agarose stamp soaked in basic solution is put in contact with a PEI/GO thin film that causes the LbL film to be etched in the areas it contacts.

5.2.3 WETS Patterning and Reduction of LbL Assemblies

PEI/GO LbL assemblies were patterned by exposing substrates to patterned agarose stamps soaked in NaOH solutions of varying basicity. To create patterned stamps for WETS, agarose was first dissolved in hot water as a 5 wt% solution. The viscous agarose solution was poured into a custom machined aluminum mold and the agarose is allowed to cool and set into a firm hydrated gel. The stamps were then immersed in solutions of 0.01, 0.03, 0.05, or 0.1 M NaOH for a minimum of 24 hours. Immediately prior to use, stamps were removed and their surface was dried with filtered air. In a typical WETS operation, the stamp was placed in contact with

the LbL assembly coated on glass for 1, 5, 10, 20, 40, or 60 min. After the stamp was removed, LbL assemblies were immediately washed with DI water and dried with filtered air. A schematic of this process is shown in Figure 5.1(c).

5.2.4 Thin Film Characterization

Thickness of PEI/GO LbL assemblies on silicon was measured with a KLA-Tencor P6 profilometer (Milpitas, CA). Sheet resistance was measured using a Signatone four point probe (Gilroy, CA), Keithley Instruments 2000 multimeter (Solon, OH), and Agilent E3644A DC power supply (Santa Clara, CA) controlled with a home-built LabView program. Prior to electrical resistivity measurements, all PEI/GO assemblies were thermally reduced in air at 175 °C for 90 minutes. Scanning electron microscopy (SEM) and energy dispersive x-ray spectroscopy (EDS) mapping was performed using a JEOL JSM-7500F microscope (Tokyo, Japan). Optical microscope images were obtained using a Swift Optical Instruments, Inc. M27LED stereo microscope (Schertz, TX).

5.3 Results and Discussion

5.3.1 pH-Dependent Growth of GO Multilayers

Solution pH is known to influence the amount of each polyelectrolyte component deposited in layer-by-layer coatings.[30,151,169] In the case of graphene oxide, pH alters its dispersion stability,[170] which alters its LbL deposition. Zeta potential of aqueous GO dispersions was measured as a function of pH, as shown in Figure 5.2. Graphene oxide is a nanoplatelet containing carboxylic acid functionality,[117] so it has low surface charge at pH < 3 due to the acid groups being mostly protonated. As the pH is increased to ≥ 6, GO reaches full deprotonation, and its zeta potential remains constant at $\sim$ -30 mV. This behavior is expected because the pK_a value for the carboxylic acid group is estimated to be 4.3.[171] It should be noted that GO dispersions

in which pH was adjusted below 2.75 became unstable after a short time (< 1 min), so they could not be used for LbL growth.

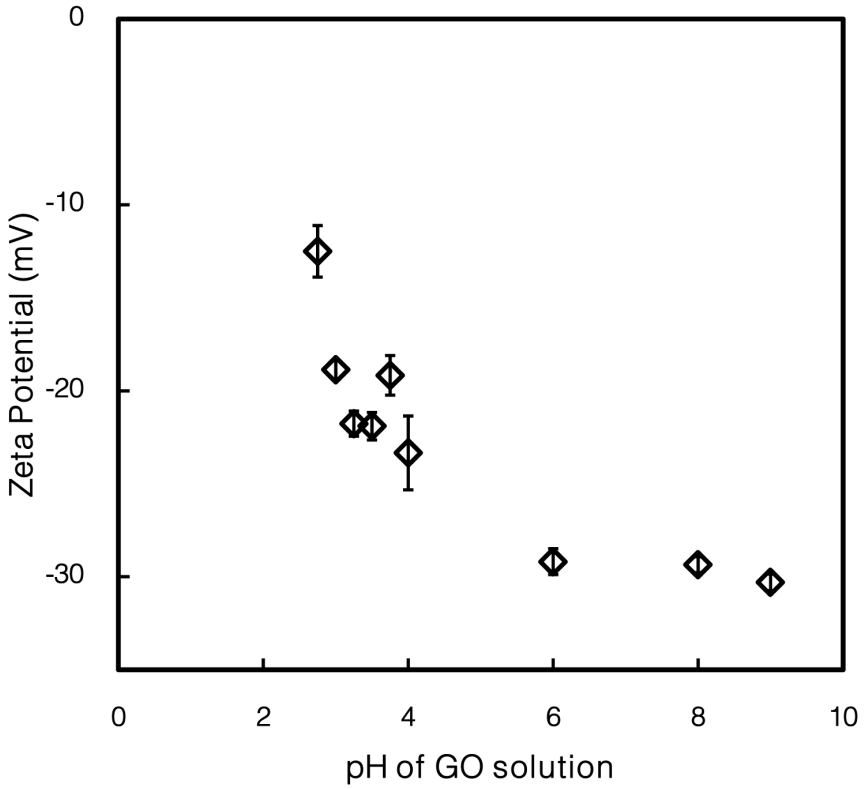

Figure 5.2: Zeta potential of aqueous graphene oxide dispersions as a function of pH. GO becomes more negatively charged as pH is increased above its pK_a ($\sim$4.3) due to deprotonation of carboxylic acid groups.

Growth of polyethyleneimine-graphene oxide layer-by-layer assemblies was carried out with varying GO dispersion pH in an effort to determine the influence of particle charge on its ability to grow. The pH of the PEI solution was held constant at 10. The profilometer thickness of 20 BL PEI/GO assemblies is shown in Figure 5.3. The thickness of these films is directly proportional to the magnitude of the GO zeta

potential. Although higher particle charge is observed at high pH, which is favorable for traditional electrostatic LbL growth,[17] particle-particle repulsion in the GO and low charge density of the previously deposited PEI layer lead to relatively poor GO adsorption. At low pH, despite the tendency of GO to aggregate, hydrogen bonding interactions between GO and PEI are favorable and greater growth results.[169] This explains the thick growth from pH 2.75 GO dispersions (14.4 nm/BL) and very thin bilayers observed at pH 9 (1.5 nm/BL).

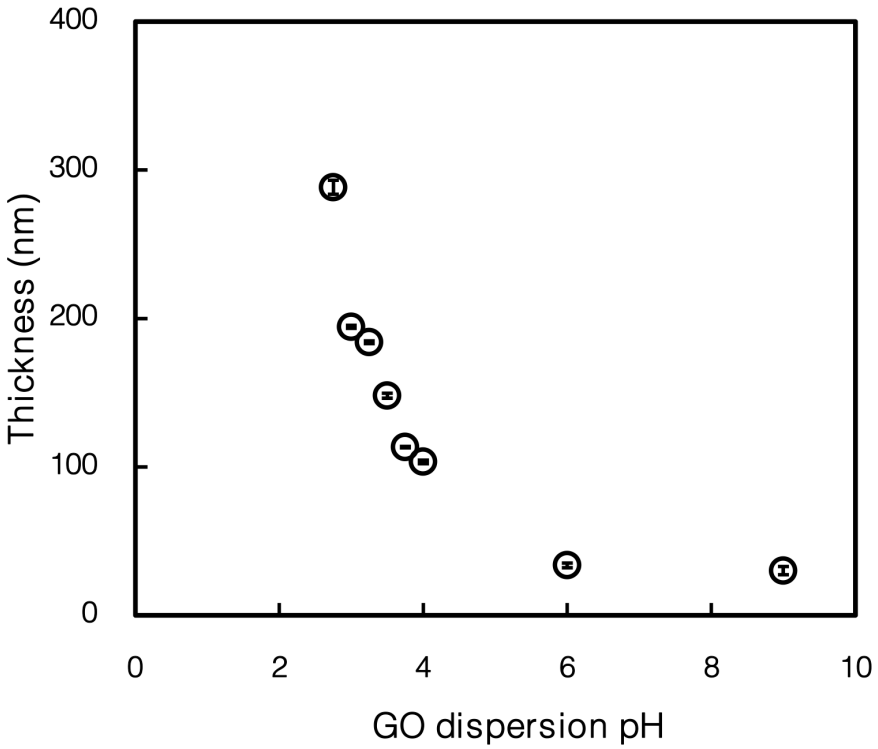

Figure 5.3: Film thickness of 20 BL PEI/GO assemblies as a function of graphene oxide dispersion pH, which correlates linearly with the trend observed for zeta potential.

5.3.2 Influence of GO Deposition pH on Electrical Resistivity

Four point probe resistivity was measured on the PEI/GO bilayers after reduction at 175 °C for 90 min. This thermal treatment has previously been shown to adequately reduce the GO in these assemblies to produce electrical conductivity.[99] The sheet resistance for 20 BL PEI/GO, as a function of GO dispersion pH, is shown in Figure 5.4. Sheet resistance is observed to be inversely proportional to the thickness of these assemblies. The pH of the GO dispersion is the only processing parameter altered between these films, suggesting it is responsible for the amount of GO deposited on the substrate. As pH is reduced from 4 to 2.75, sheet resistance decreases nearly two orders of magnitude.

5.3.3 WETS Patterning of GO-Based LbL Assemblies

LbL films have a tendency to degrade or detach in the presence of high or low pH or high ionic strength solutions,[153,154] so WETS was employed by charging agarose stamps with basic solution to intentionally and selectively destabilize portions of the film. This technique has already been shown to successfully pattern poly(allylamine hydrochloride)/poly(acrylic acid) multilayers with 10 µm half-pitch. A variety of base concentrations and exposure times were investigated to determine the extent of etching possible using this wet stamping technique. Figure 5.5 shows optical micrographs of PEI/GO films after WETS etching for 1, 5, 10, 20, 40, and 60 minutes using 0.01, 0.03, 0.05, and 0.1 M NaOH solutions. This etching was initially applied to films deposited from GO dispersions without pH alteration (pH $\sim$ 3.25).

Based on the images in Figure 5.5, base concentration was determined to be the key variable driving film etching. Additionally, the etch appears to be binary (i.e. the film was either removed from the substrate or it was not). Some basicity threshold between 0.01 and 0.03 M was necessary for the etching of PEI/GO to occur.

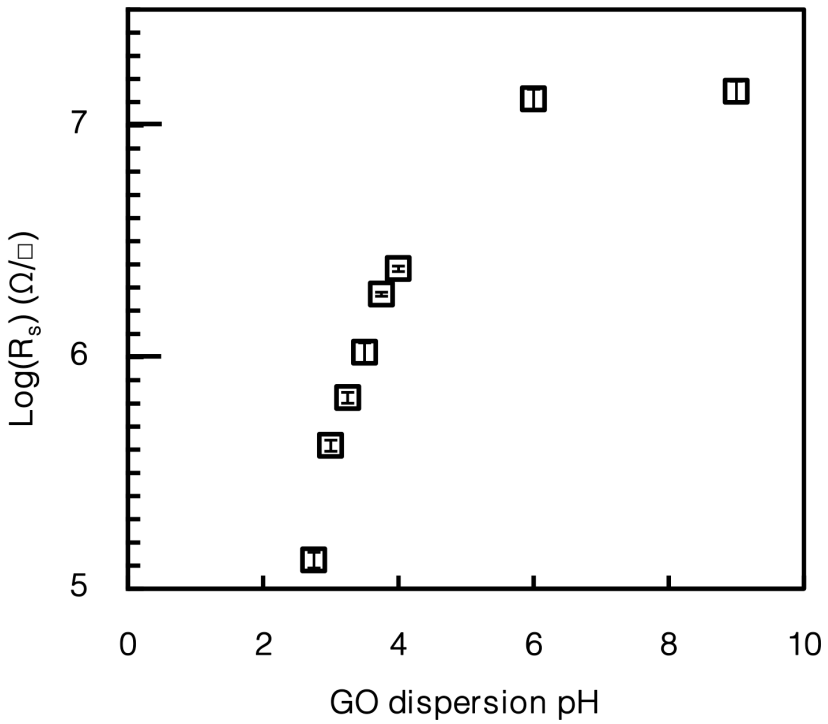

Figure 5.4: Sheet resistance (R_s) of 20 BL PEI/GO assemblies as a function of GO dispersion pH. The dispersion pH is inversely proportional to PEI/GO assembly thickness and GO zeta potential.

Once this threshold concentration has been reached, the film is readily etched, even with exposure time as short as one minute (slightly longer with 0.03 M NaOH). It is important to note that longer exposure times do not necessarily lead to more complete etching. As the 0.03 and 0.05 M stamps reached etching times of 40 and 60 min., the resolution of the rectangular features was lost. At these long time intervals, it is known that there is drying of the stamps and etchant in contact with the substrate. As the etchant solution dries, its efficacy is lost, and the exposed areas are unaffected. This unintentional result may allow for correction of the etch procedure, if necessary, as the dried etchant can be rinsed off with water, and the PEI/GO film can be re-exposed. Etching with 0.1 M NaOH effectively removed

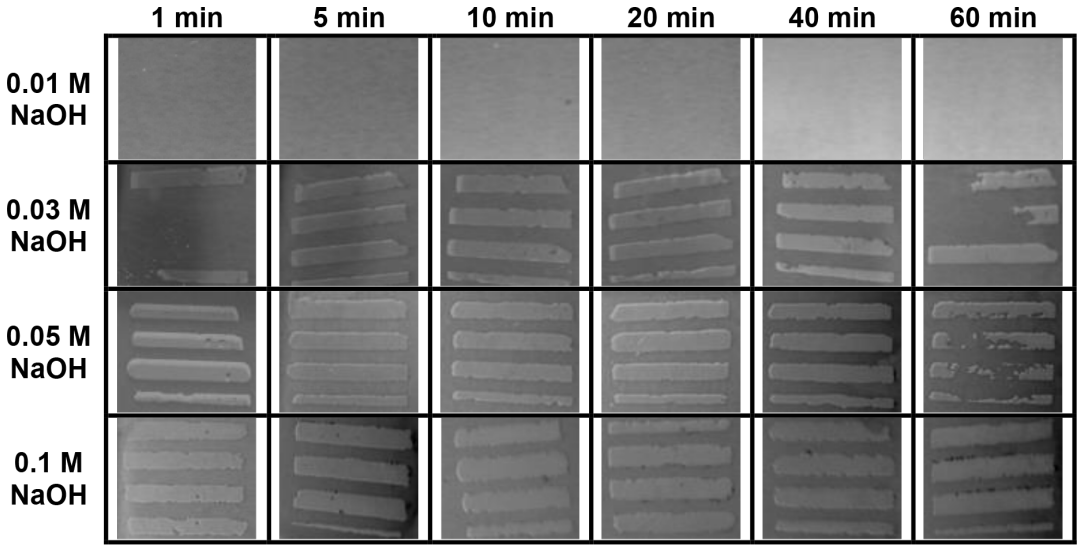

Figure 5.5: Optical micrographs of PEI/GO assemblies made from GO dispersions with unaltered pH (3.25). These films were removed from their glass substrate using agarose stamps swollen with sufficiently basic solution ($\geq$ 0.03 M NaOH), but over-etching occurs when the basicity is too high and the stamp has been in contact too long. Feature dimensions shown are approximately 2 x 10 mm.

material, but led to larger than desired areas of film being removed due to over-etching, which becomes apparent beyond 5 min.

WETS etching of the most conductive assemblies, created with a pH 2.75 GO dispersion, was also examined. Optical micrographs of etched films are shown in Figure 5.6. These PEI/GO assemblies showed slightly greater etch resistance in terms of both base concentration and exposure time. Although 0.05 M NaOH was able to etch most of the pattern after 60 min of exposure, only 0.1 M NaOH was capable of completely etching the pattern from the stamp. After 40 min of etching, signs of over-etching appear, but to a lesser degree relative to assemblies formed from GO dispersions with unaltered pH. The greater etch resistance of these assemblies is most likely due to greater film thickness (288 nm from pH 2.75 dispersions and 184 nm from unaltered pH 3.25 dispersions).

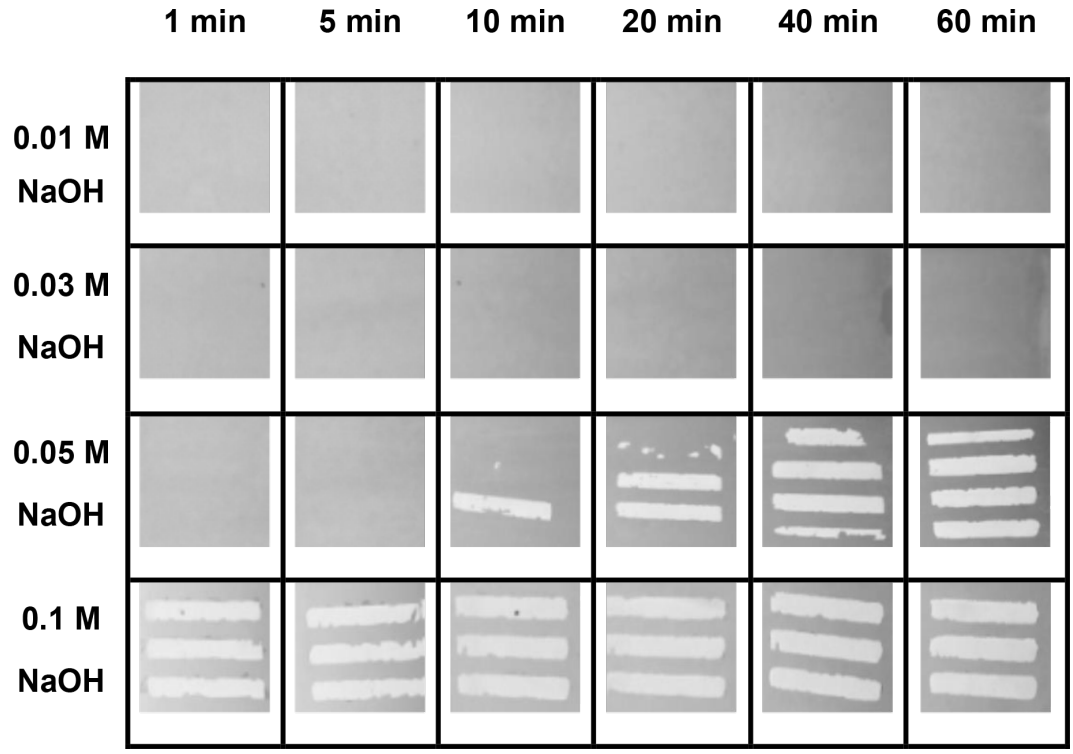

Figure 5.6: Optical micrographs of PEI/GO assemblies made from GO dispersions altered to pH 2.75 and wet stamped with base-swollen agarose stamps. Greater film thickness at this pH level requires higher basicity solutions to etch the film. Feature dimensions shown are approximately 2 x 10 mm.

5.3.4 Quality of PEI/GO Etching

The difference between etched and unetched regions (i.e. quality of the etch) is of great importance for electronics applications. For this reason, these differences were carefully analyzed by ATR-FTIR, SEM, EDS, and four point probe resistivity. ATR-FTIR is sensitive to the 20BL LbL assembly formed from an unaltered GO dispersion, as shown in Figure 5.7. The LbL assembly displays carbonyl and broad carboxylic acid absorption at 1610 and $\sim$3300 cm^{-1}, respectively, which are not observed for bare glass. When the film is etched from the glass substrate, the two absorptions disappear and the spectrum is identical to pristine glass. SEM imaging and EDS

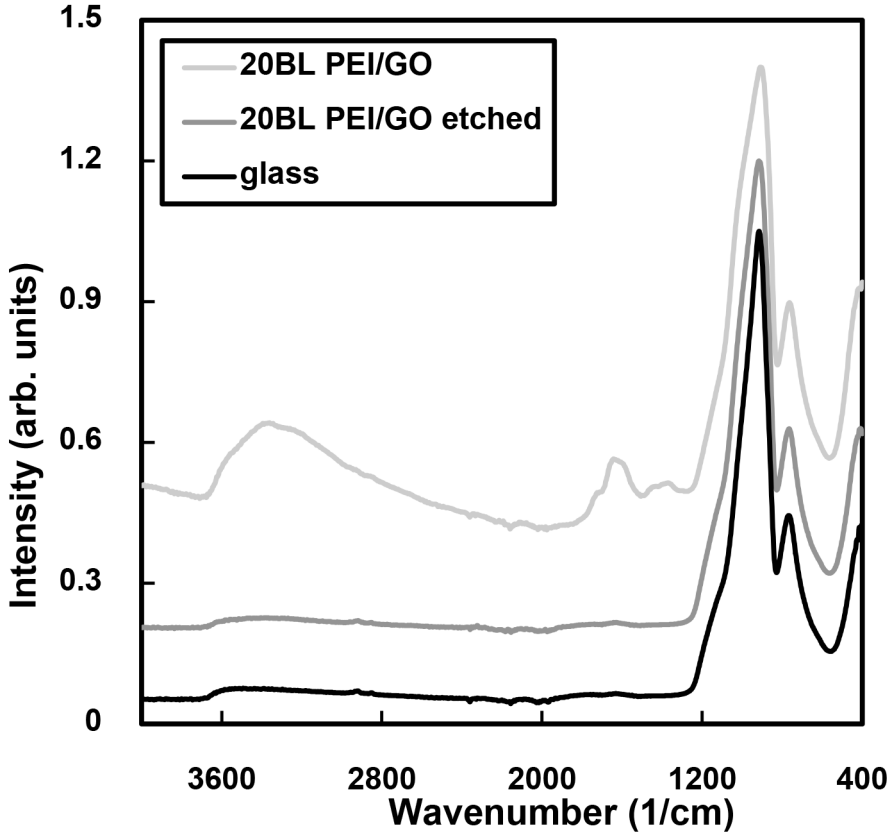

Figure 5.7: ATR-FTIR spectra of glass, 20 BL PEI/GO deposited on glass, and 20 BL PEI/GO deposited on glass and then etched away. The 20 BL PEI/GO assembly shows additional absorption peaks at ∼3300 and 1610 cm^{-1} (not present for glass), but the etched film shows none of these additional features. This suggests complete etching of the film, with little or no material left on the glass substrate.

mapping of the same assembly, shown in Figure 5.8, was employed to investigate the etched/unetched areas of the film at a microscopic level. Conductivity differences between the film (dark, Fig. 5.8(a)) and substate glass in the etched region (light) are very apparent, and little or no film remains in the exposed area. At a finer scale (Fig. 5.8(c)), the lack of surface features caused by GO in the film in the exposed region on the left contrasts strongly with the unexposed film on the right. Further evidence of the etch quality is observed in C K_α EDS mapping (Fig. 5.8(b, d)), which displays

regions of high (bright) and low (dark) carbon content in the film. Four point probe resistivity measurements indicated resistance higher than the detection range of the instrument for etched areas. The resistivity of unexposed regions was unchanged ($\sim 10^5\ \Omega/\square$), as was the resistivity of areas exposed during WETS that were insufficient to remove the film.

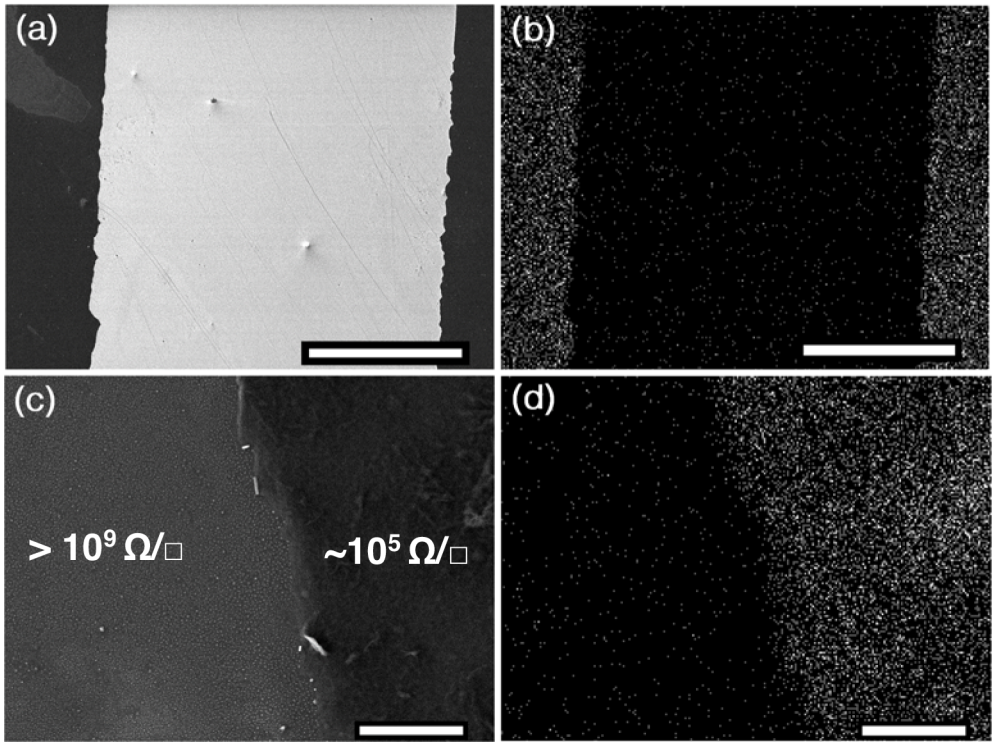

Figure 5.8: Low magnification (1 mm scale bar) SEM (a) and EDS C K_α (b) images of an etched stripe with unetched film on either side. The EDS map shows low carbon signal in the etched region relative to the unetched region. At high magnification (5 µm scale bar), the rough surface of the film is visible in SEM (c, right side), and the EDS C K_α map (d) again shows low carbon signal from the etched region. Sheet resistance of etched and unetched regions are shown in (c).

5.4 Conclusions

The ability to pattern electrically conductive layer-by-layer films has been demonstrated using a relatively safe and simple wet stamping methodology. Because of the sharp drop in charge density of graphene oxide platelets near their pK_a, LbL processing allows significant tailoring of layer thickness and resistance, with growth ranging from 1.5–14.4 nm/BL, and sheet resistance spanning three orders of magnitude, 10^5–10^7 $\Omega/\square$, after thermal reduction. Using a relatively dilute concentration of basic etchant solution, these films are quickly removed to form a patterned conductive layer using the WETS process. The wet stamping process used with basic solution produces a good quality pattern, with little or no material left in etched regions, ensuring no short circuiting of patterned conductive layers. Furthermore, dried etchant solution can be removed with little influence on the film, which imparts the ability to correct the etching process. With additional refinement, these LbL assemblies could be used to produce patterned circuits on a variety of substrates with a high degree of control and tailorability, offering the potential for environmentally-friendly processing of organic electronics.

VI. CONCLUSIONS AND FUTURE WORK

6.1 Barrier and Conductivity in Platelet-Based Thin Film Assemblies

The goal of this research was to investigate how platelet particles can contribute to gas barrier and electrical properties of thin films. Through layer-by-layer processing of water-soluble (or dispersible) ingredients, these thin films were able to be constructed into self-assembled, aligned layers that are capable of blocking oxygen gas in both dry and humid conditions. If the films contain graphene oxide, a simple heat treatment produces electrical conductivity as well. This work illustrates the versatility of layer-by-layer fabrication and the ease with which this technique can create materials for multiple functions at once.

6.1.1 Influence of Film Density on Gas Barrier Films

In order to examine density of films prepared using layer-by-layer assembly, comparison needed to be made between films that were otherwise similar in microstructure and composition. Toward this goal, pyrene functionality was introduced as a side group onto PEI, which was then grown in quadlayers with PAA and MMT. PEI was modified by reacting the neat polymer with pyrene carboxaldehyde and sodium borohydride, which bonds the pyrene to the PEI chains through reductive elimination and does not introduce any other functional groups, as indicated by FTIR. As the pyrene groups are known to have strong hydrophobic interactions with each other, they force PEI to coil, which leads to increased deposition density (1.45 g/cm^3 for PEI-Py vs. 1.24 g/cm^3 for PEI, as measured by QCM) despite having similar profilometer thickness to films constructed with neat PEI. Oxygen permeation of both films deposited on PET was compared, with the denser films realizing more than an order of magnitude decrease in OTR and permeability for 3 quadlayers (0.75 to 0.059

$cm^3/m^2/day/atm$). A graphical summary of these films is shown in Figure 6.1. This study demonstrated the importance of film density to gas barrier thin films, which is fundamental in understanding how to create better barriers.

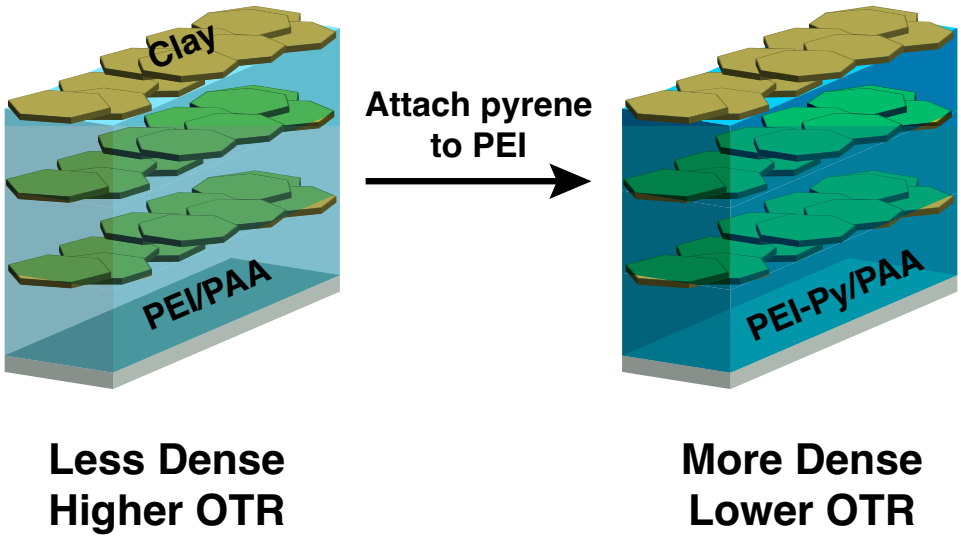

Figure 6.1: Schematic of research in Chapter 3, where pyrene-labeled PEI was used to produce denser polymer layers in LbL assemblies. This resulted in decreased OTR compared with films of similar thickness and number of layers containing neat PEI.

6.1.2 Gas Barrier and Electrical Conductivity in Reduced Graphene Oxide-Based Films

The influence of thermal reduction of GO on barrier and electrical conductivity in thin films was investigated. GO, produced from chemical oxidation of graphite powder, and PEI were layered using LbL assembly. Thermal reduction of GO as a function of reducing time and temperature were monitored by XPS and electrical sheet resistance measurements, which indicated GO begins reducing in air above 150 °C. As the GO reduces, electrical resistivity drops at least 5 orders of magnitude,

and XPS measurements indicate that the GO loses much of its sp^3 carbon content and gains graphitic sp^2 carbons. Cross sections viewed under TEM and topography viewed under SEM indicate a dense, oriented film of GO flakes in polymer, which provides a highly tortuous pathway for gas permeation. In high humidity conditions, unreduced films are believed to swell, resulting in relatively high OTR. Thermal reduction of GO decreases both hydrophilicity and film thickness. The resulting compacted structure is has less free volume for gas diffusion and is less susceptible to swelling. Though both unreduced and reduced films have similar high resistance to gas permeation in low humidity conditions, only the reduced films are capable of retaining barrier in high humidity conditions (summarized in Figure 6.2). This study presents the high barrier at all ambient conditions, and the best polymer composite barrier film at this time.

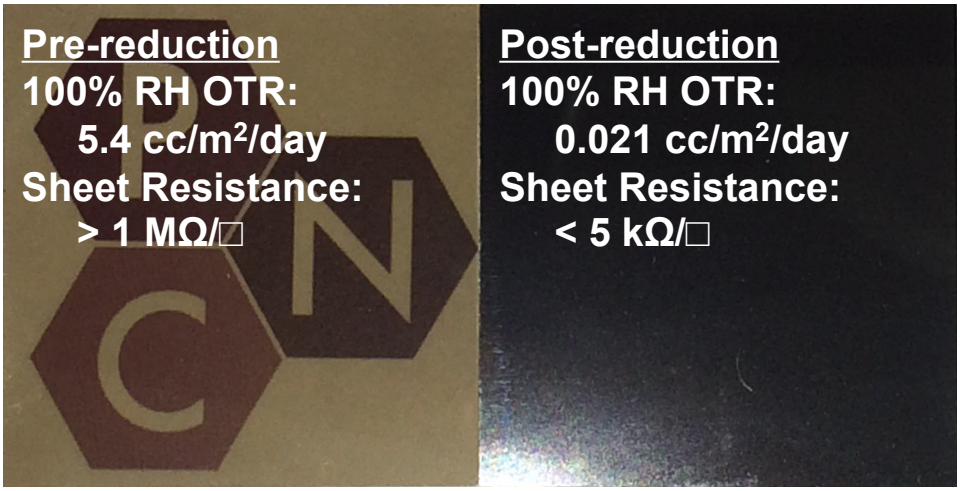

Figure 6.2: Summary of work presented in Chapter 4. GO, in LbL films with PEI, was thermally reduced to produce electrically conductive films that retain O_2 barrier under both dry and humid conditions.

6.1.3 Patterning of GO-based Assemblies Through Soft Lithography

The ability to pattern films of GO and PEI using soft lithography was examined. Once thermally reduced, these patterns could be used for flexible electronics connections, e.g. To gather some information about how to best realize conductive patterns, the pH of GO deposition solutions was optimized to deliver the highest content of GO, ensuring the best conductivity of the assembly after reduction. Zeta potential measurement revealed that more GO deposits when it has a nearly neutral charge, indicating thick growth occurs via hydrogen bonding with PEI. Four point probe electrical resistivity indicates a two order of magnitude improvement in conductivity when the pH of the GO solution is dropped to pH 2.75 from pH 6 or above. Patterns were etched into the deposited films by creating patterned stamps in water-swellable agarose gel, swelling the stamps with mildly basic NaOH solution, and using these stamps to selectively wet etch the film down to the substrate. After thermal reduction, patterned surfaces decreased in electrical sheet resistance by at least two orders of magnitude. The etch procedure produced complete etching of the film—no traces of the film could be detected in etched regions using FT-IR and SEM/EDS. Complete etching of the films in selected areas is essential for circuits, for instance, as incomplete etching results in short circuiting. A graphical summary of this work is shown in Figure 6.3. This technique can easily be accomplished in ambient conditions without the need for UV light filters or photoresist.

6.2 Future Studies

From the previous three chapters, it has been shown that graphene oxide can act in role as both an oxygen barrier and electrical conductor. Though seemingly unrelated, the marriage of these two properties could have important industrial applications. As processing of these water soluble ingredients into an oriented film

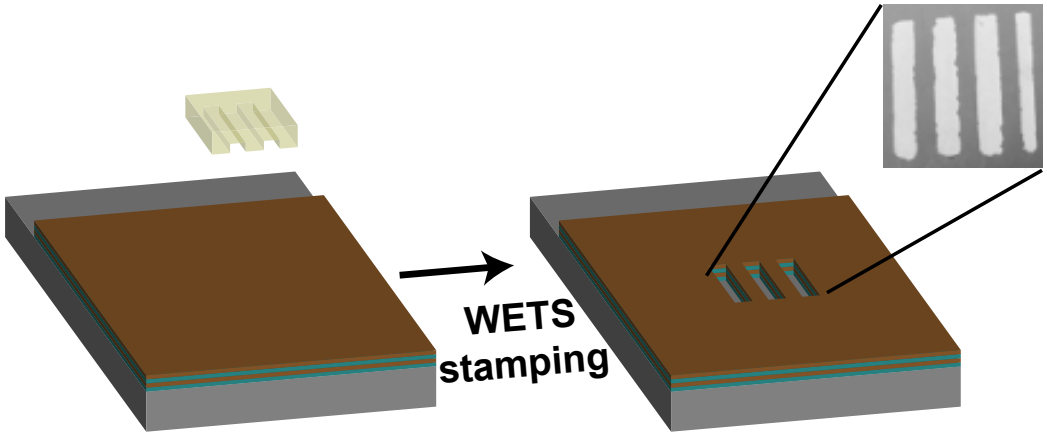

Figure 6.3: Schematic of research presented in Chapter 5. PEI/GO LbL films were patterned using wet etching stamping (WETS) from agarose stamps containing mildly basic solution, resulting in complete removal of the film. Upon thermal reduction, these patterns became electrical conductors.

is both easy and environmentally benign, furthering the commercial attractiveness of its capabilities is important in establishing it as a viable industrial alternative to competing technologies. Better flexible conductive films will be of increased interest as the flexible electronics market grows, an area where LbL processing could contribute greatly.

6.2.1 Damage Detection in Conductive Barrier Thin Films

Detection of damage to gas barrier layers is industrially relevant for reactors under high pressure and to medical devices.[172] It is currently difficult to detect if gases are being blocked or retained, as small leaks resulting from damage are difficult to detect. Because polymer/rGO films are electrical conductors, damage detection of these barrier films is possible. Scratches, pinholes, and cracking, for instance, will lead to increases in the electrical resistance of the film. Furthermore, locating the damage is also feasible when an array of electrodes is placed around the film. When the film is

damaged (resulting in loss of barrier properties), electrodes with an electrical path over the damaged area will increase in resistance, as the current has a greater distance to travel through moderately resistive material, (illustrated in Figure 6.4). With a crosslinkable polyelectrolyte, minor damage could be avoided altogether. In order to study this, LbL films of polyvinylamine (PVAm), which is more easily crosslinked, and GO can be created and reduced. They would then tested for barrier properties before and after scratching (both with and without glutaraldehyde crosslinking). Placing an electrode array on the sample provides many electrical resistance test points, from which it will be possible to determine damage location.

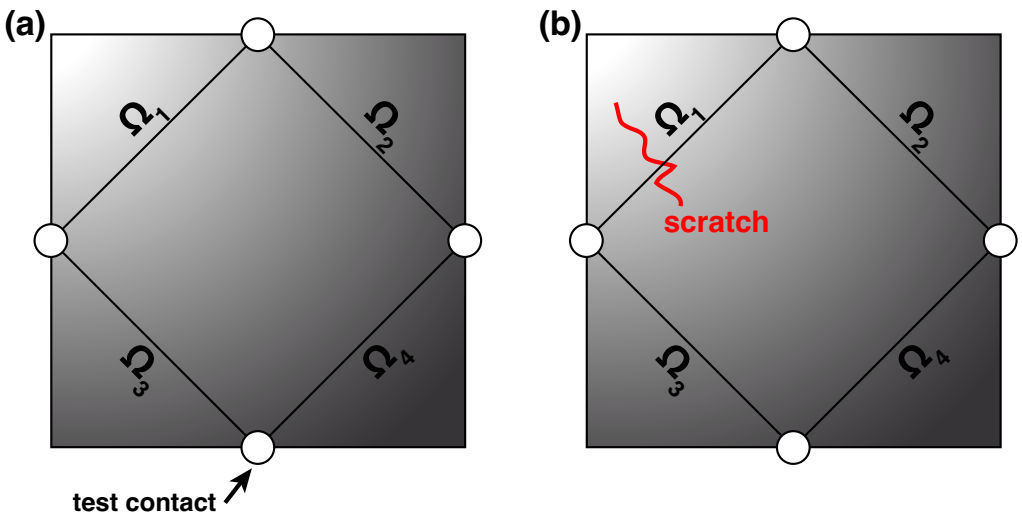

Figure 6.4: Proposed layout of electrodes for locating damage to a conductive barrier film. Without damage (a), the resistance between contacts is approximately equivalent, $\Omega_1 = \Omega_2 = \Omega_3 = \Omega_4$. When the film is damaged (b), resistance between the two contacts where the damage is located will be substantially higher than between other contacts, $\Omega_1 > \Omega_2 = \Omega_3 = \Omega_4$

6.2.2 PEI-Py/graphene and GO films

Pyrene is known to have strong intermolecular interactions with graphene sheets, which allows graphene to be stabilized in solution.[173–175] Extending work from Chapters 3 and 4, PEI-Py could be used to stabilize graphene in an aqueous suspension, which could then be layered with graphene oxide. With its pyrene moiety, PEI-Py is uniquely capable of attaching to the surface of graphene sheets via π–π interactions. In water, this is realized by ultrasonication of the graphene flakes in the presence of stabilizer. Sonication temperarily disrupts bonding between sheets, which allows PEI-PY to more permanently attach to the surface of the sheets, shown schematically in Figure 6.5. As the PEI-Py has been shown to behave similar in LbL deposition to neat PEI, a polycation, it could easily be layered with anionic GO. The resulting films would contain a much higher content of platelets and conductive filler in few deposited layers, opening up the possiblity for increased electrical conductivity and barrier to water vapor.

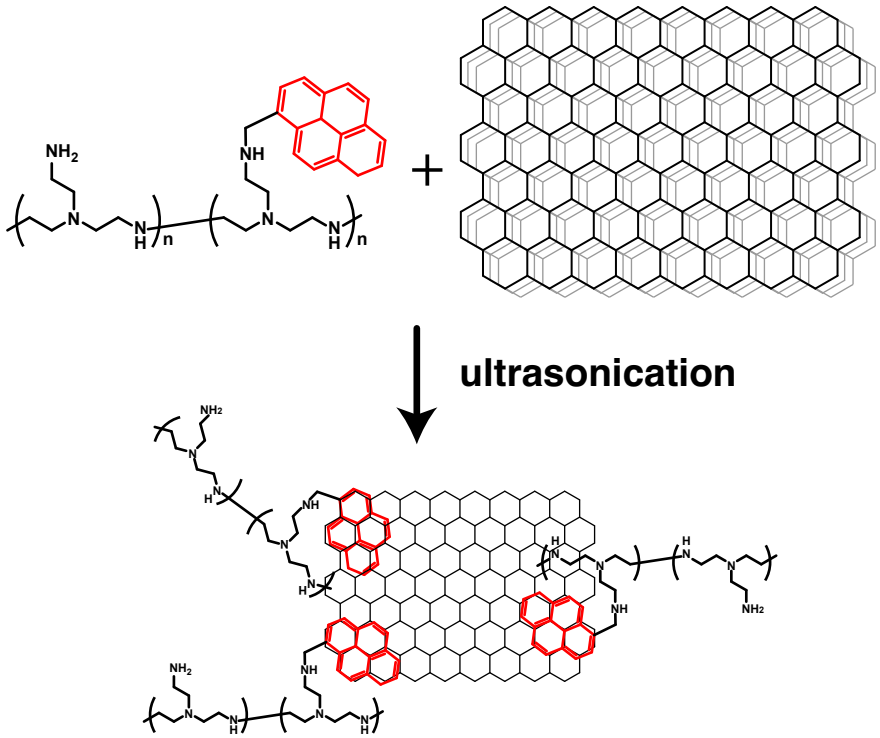

Figure 6.5: Pyrene functionality from PEI-Py is capable of non-covalent bonding with graphene sheets upon ultrasonication, resulting in a water-based suspension of graphene. The resulting suspension can be used in LbL processing in the same way as neat PEI.

6.2.3 Improved Patterning Resolution

Though soft patterning of conductive LbL films has been shown in Chapter 5, further studies are needed to refine the process and reduce the size of patterned features. In order to realize this goal, smaller features must be present in the stamps. With the increase in popularity of focused ion beam (FIB) systems, it is now possible to create highly customized stamp masters from which soft lithography stamps can be cast, as shown in Figure 6.6.

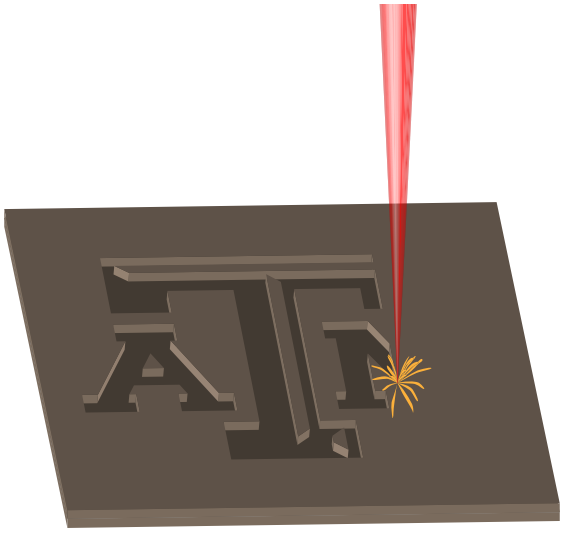

Figure 6.6: A schematic of FIB patterning, a process in which a beam of ions directly writes a pattern into a substrate. FIB has resolution below 10 nm, and the patterns it creates on hard substrates such as Si can be used as stamp masters for soft lithography.

FIB is routinely used to rapidly create sub-micron features in silicon, which allows it to be used for this purpose. In order to study the effects of miniaturization of features, a systematic approach to reducing feature size is needed, with a progression from 10 µm to 1 µm to sub micron feature sizes. This work can then be extended to creating multilevel semiconductor devices by repeated deposition—reduction—patterning cycles (Figure 6.7), similar to how features are currently created on silicon. This is necessary for the development of field effect transistors, photonics, and microelectromechanical systems.

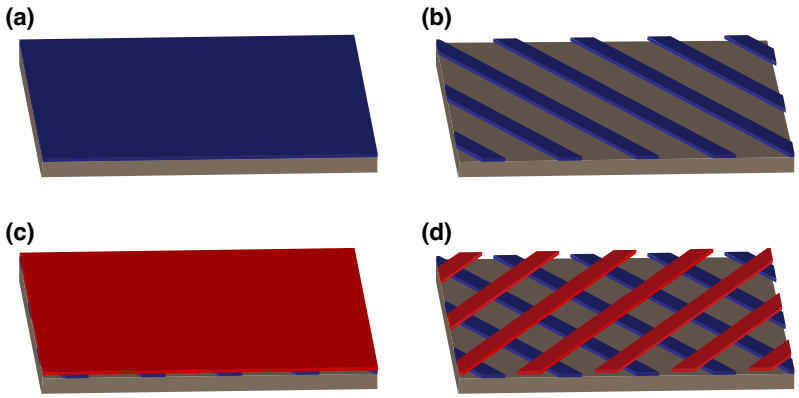

Figure 6.7: A GO/polymer LbL film is deposited (a) and patterned using soft lithography followed by reduction. A second GO-based assembly is deposited on top of the first patterned layer (c), which can then be patterned and reduced (d) to form complex structures. Higher resistance to etching after reduction ensures previously deposited patterns are not altered.

REFERENCES

(1) Lupinski, J. H.; Moore, R. S. *ACS Symp. Ser.* **1989**, *407*, 1–25.

(2) Kolosov, D.; English, D. S.; Bulovic, V.; Barbara, P. F.; Forrest, S. R.; Thompson, M. E. *J. Appl. Phys.* **2001**, *90*, 3242–3247.

(3) Burrows, P. E.; Bulovic, V.; Forrest, S. R.; Sapochak, L. S.; Mccarty, D. M.; Thompson, M. E. *Appl. Phys. Lett.* **1994**, *65*, 2922–2924.

(4) Kamp, M.; Bartsch, J.; Nold, S.; Retzlaff, M.; Horteis, M.; Glunz, S. W. *Energy Procedia* **2011**, *8*, 558–564.

(5) Affinito, J. D.; Gross, M. E.; Coronado, C. A.; Graff, G. L.; Greenwell, E. N.; Martin, P. M. *Thin Solid Films* **1996**, *290*, 63–67.

(6) Yanaka, M.; Henry, B. M.; Roberts, A. P.; Grovenor, C. R. M.; Briggs, G. A. D.; Sutton, A. P.; Miyamoto, T.; Tsukahara, Y.; Takeda, N.; Chater, R. J. *Thin Solid Films* **2001**, *397*, 176–185.

(7) Roberts, A. P.; Henry, B. M.; Sutton, A. P.; Grovenor, C. R. M.; Briggs, G. A. D.; Miyamoto, T.; Kano, A.; Tsukahara, Y.; Yanaka, M. *J. Membr. Sci.* **2002**, *208*, 75–88.

(8) Mercea, P.; Muresan, L.; Mecea, V. *J. Membr. Sci.* **1985**, *24*, 297–307.

(9) Jamieson, E. H. H.; Windle, A. H. *J. Mater. Sci.* **1983**, *18*, 64–80.

(10) Petit, S.; Laurens, P.; Barthes-Labrousse, M. G.; Amouroux, J.; Arefi-Khonsari, F. *J. Adhes. Sci. Technol.* **2003**, *17*, 353–368.

(11) Larciprete, R.; Fabris, S.; Sun, T.; Lacovig, P.; Baraldi, A.; Lizzit, S. *J. Am. Chem. Soc.* **2011**, *133*, 17315–17321.

(12) IPC: Ipc 2221 Generic Standard on Printed Board Design., Standard, 2012.

(13) LaDou, J. *Int. J. Hyg. Environ. Health* **2006**, *209*, 211–219.

(14) Huang, K.; Guo, J.; Xu, Z. M. *J. Hazard. Mater.* **2009**, *164*, 399–408.

(15) McGuire, G. E., *Semiconductor Materials and Process Technology Handbook*; William Andrew Publishing/Noyes: Westwood, NJ, 1988.

(16) Lin, S. H.; Kiang, C. D. *J. Hazard. Mater.* **2003**, *97*, 159–171.

(17) Decher, G.; Schlenoff, J. B., *Multilayer Thin Films Sequential Assembly of Nanocomposite Materials*; Wiley-VCH: Weinheim, Germany, 2012.

(18) Ariga, K.; Ji, Q.; Hill, J. P.; Bando, Y.; Aono, M. *NPG Asia Mater.* **2012**, *4*, e17.

(19) Bertrand, P.; Jonas, A.; Laschewsky, A.; Legras, R. *Macromol. Rapid Commun.* **2000**, *21*, 319–348.

(20) Caridade, S. G.; Monge, C.; Gilde, F.; Boudou, T.; Mano, J. F.; Picart, C. *Biomacromolecules* **2013**, *14*, 1653–1660.

(21) Dam, H. H.; Caruso, F. *Langmuir* **2013**, *29*, 7203–7208.

(22) Kastl, L.; Sasse, D.; Wulf, V.; Hartmann, R.; Mircheski, J.; Ranke, C.; Carregal-Romero, S.; Martinez-Lopez, J. A.; Fernandez-Chacon, R.; Parak, W. J.; Elsasser, H. P.; Rivera Gil, P. *ACS Nano* **2013**, *7*, 6605–6618.

(23) Poon, Z.; Lee, J. B.; Morton, S. W.; Hammond, P. T. *Nano Lett.* **2011**, *11*, 2096–103.

(24) Robert, C.; Feller, J. F.; Castro, M. *ACS Appl. Mater. Interfaces* **2012**, *4*, 3508–3516.

(25) Aoki, P. H. B.; Alessio, P.; Furini, L. N.; Constantino, C. J. L.; Neves, T.; Paulovich, F. V.; de Oliveira, M. C. F.; Oliveira, O. N. *Langmuir* **2013**, *29*, 7542–7550.

(26) Shen, L.; Wang, B.; Wang, J.; Fu, J.; Picart, C.; Ji, J. *ACS Appl. Mater. Interfaces* **2012**, *4*, 4476–4483.

(27) Wang, D.; Liu, N.; Xu, W. L.; Sun, G. *J. Phys. Chem. C* **2011**, *115*, 6825–6832.

(28) Laufer, G.; Kirkland, C.; Morgan, A. B.; Grunlan, J. C. *ACS Macro Lett.* **2013**, *2*, 361–365.

(29) Apaydin, K.; Laachachi, A.; Ball, V.; Jimenez, M.; Bourbigot, S.; Toniazzo, V.; Ruch, D. *Polym. Degrad. Stab.* **2013**, *98*, 627–634.

(30) Shiratori, S. S.; Rubner, M. F. *Macromolecules* **2000**, *33*, 4213–4219.

(31) Garg, A.; Heflin, J. R.; Gibson, H. W.; Davis, R. M. *Langmuir* **2008**, *24*, 10887–10894.

(32) Priolo, M. A.; Holder, K. M.; Greenlee, S. M.; Stevens, B. E.; Grunlan, J. C. *Chem. Mater.* **2013**, *25*, 1649–1655.

(33) Priolo, M. A.; Holder, K. M.; Gamboa, D.; Grunlan, J. C. *Langmuir* **2011**, *27*, 12106–12114.

(34) Yang, Y. H.; Bolling, L.; Priolo, M. A.; Grunlan, J. C. *Adv. Mater.* **2013**, *25*, 503–508.

(35) Kotov, N. A.; Dekany, I.; Fendler, J. H. *Adv. Mater.* **1996**, *8*, 637–641.

(36) Iler, R. K. *J. Am. Ceram. Soc.* **1964**, *47*, 194–198.

(37) Iler, R. K. *J. Colloid Interface Sci.* **1966**, *21*, 569–594.

(38) Decher, G.; Hong, J. D. *Makromol. Chem., Macromol. Symp.* **1991**, *46*, 321–327.

(39) Decher, G.; Hong, J. D. *Ber. Bunsen-Ges.* **1991**, *95*, 1430–1434.

(40) Decher, G. *Science* **1997**, *277*, 1232–1237.

(41) Yoo, D.; Shiratori, S. S.; Rubner, M. F. *Macromolecules* **1998**, *31*, 4309–4318.

(42) Decher, G.; Schmitt, J. In *Trends in Colloid and Interface Science Vi*, Helm, C., Lsche, M., Mhwald, H., Eds.; Progress in Colloid & Polymer Science, Vol. 89; Steinkopff: 1992; Chapter 36, pp 160–164.

(43) Losche, M.; Schmitt, J.; Decher, G.; Bouwman, W. G.; Kjaer, K. *Macromolecules* **1998**, *31*, 8893–8906.

(44) Ruths, J.; Essler, F.; Decher, G.; Riegler, H. *Langmuir* **2000**, *16*, 8871–8878.

(45) Lvov, Y.; Decher, G.; Mohwald, H. *Langmuir* **1993**, *9*, 481–486.

(46) Buscher, K.; Graf, K.; Ahrens, H.; Helm, C. A. *Langmuir* **2002**, *18*, 3585–3591.

(47) Tan, H. L.; McMurdo, M. J.; Pan, G. Q.; Van Patten, P. G. *Langmuir* **2003**, *19*, 9311–9314.

(48) Borges, J.; Mano, J. F. *Chem. Rev.* **2014**, *114*, 8883–8942.

(49) Stockton, W. B.; Rubner, M. F. *Macromolecules* **1997**, *30*, 2717–2725.

(50) Fu, Y.; Chen, H.; Qiu, D. L.; Wang, Z. Q.; Zhang, X. *Langmuir* **2002**, *18*, 4989–4995.

(51) Zhang, H. Y.; Fu, Y.; Wang, D.; Wang, L. Y.; Wang, Z. Q.; Zhang, X. *Langmuir* **2003**, *19*, 8497–8502.

(52) Zhang, H. Y.; Wang, Z. Q.; Zhang, Y. Q.; Zhang, X. *Langmuir* **2004**, *20*, 9366–9370.

(53) Decher, G.; Lehr, B.; Lowack, K.; Lvov, Y.; Schmitt, J. *Biosens. Bioelectron.* **1994**, *9*, 677–684.

(54) Shimazaki, Y.; Mitsuishi, M.; Ito, S.; Yamamoto, M. *Langmuir* **1997**, *13*, 1385–1387.

(55) Shimazaki, Y.; Mitsuishi, M.; Ito, S.; Yamamoto, M. *Macromolecules* **1999**, *32*, 8220–8223.

(56) Bourdillon, C.; Demaille, C.; Moiroux, J.; Saveant, J. M. *J. Am. Chem. Soc.* **1994**, *116*, 10328–10329.

(57) Anzai, J.; Nishimura, M. *J. Chem. Soc., Perkin Trans. 2* **1997**, 1887–1889.

(58) Lee, H.; Kepley, L. J.; Hong, H. G.; Mallouk, T. E. *J. Am. Chem. Soc.* **1988**, *110*, 618–620.

(59) Xiong, H. M.; Cheng, M. H.; Zhou, Z.; Zhang, X.; Shen, J. C. *Adv. Mater.* **1998**, *10*, 529–532.

(60) Liu, Y. L.; Bruening, M. L.; Bergbreiter, D. E.; Crooks, R. M. *Angew. Chem., Int. Ed. Engl.* **1997**, *36*, 2114–2116.

(61) Liang, Z. Q.; Wang, Q. *Langmuir* **2004**, *20*, 9600–9606.

(62) Serizawa, T.; Matsukuma, D.; Nanameki, K.; Uemura, M.; Kurusu, F.; Akashi, M. *Macromolecules* **2004**, *37*, 6531–6536.

(63) Tang, Z. Y.; Wang, Y.; Podsiadlo, P.; Kotov, N. A. *Adv. Mater.* **2006**, *18*, 3203–3224.

(64) Onda, M.; Ariga, K.; Kunitake, T. *J. Biosci. Bioeng.* **1999**, *87*, 69–75.

(65) Onda, M.; Lvov, Y.; Ariga, K.; Kunitake, T. *Biotechnol. Bioeng.* **1996**, *51*, 163–167.

(66) Ferreira, M.; Fiorito, P. A.; Oliveira, O. N.; de Torresi, S. I. C. *Biosens. Bioelectron.* **2004**, *19*, 1611–1615.

(67) Caruso, F.; Niikura, K.; Furlong, D. N.; Okahata, Y. *Langmuir* **1997**, *13*, 3427–3433.

(68) Burke, S. E.; Barrett, C. J. *Macromolecules* **2004**, *37*, 5375–5384.

(69) Wood, K. C.; Boedicker, J. Q.; Lynn, D. M.; Hammond, P. T. *Langmuir* **2005**, *21*, 1603–1609.

(70) Joseph, N.; Ahmadiannamini, P.; Hoogenboom, R.; Vankelecom, I. F. J. *Polym. Chem.* **2014**, *5*, 1817–1831.

(71) Levasalmi, J. M.; McCarthy, T. J. *Macromolecules* **1997**, *30*, 1752–1757.

(72) Sullivan, D. M.; Bruening, M. L. *Chem. Mater.* **2003**, *15*, 281–287.

(73) Kim, D.; Tzeng, P.; Barnett, K. J.; Yang, Y. H.; Wilhite, B. A.; Grunlan, J. C. *Adv. Mater.* **2014**, *26*, 746–751.

(74) Priolo, M. A.; Gamboa, D.; Grunlan, J. C. *ACS Appl. Mater. Interfaces* **2010**, *2*, 312–320.

(75) Yang, Y. H.; Haile, M.; Park, Y. T.; Malek, F. A.; Grunlan, J. C. *Macromolecules* **2011**, *44*, 1450–1459.

(76) Priolo, M. A.; Gamboa, D.; Holder, K. M.; Grunlan, J. C. *Nano Lett.* **2010**, *10*, 4970–4974.

(77) Lee, S. W.; Yabuuchi, N.; Gallant, B. M.; Chen, S.; Kim, B. S.; Hammond, P. T.; Shao-Horn, Y. *Nat. Nanotechnol.* **2010**, *5*, 531–537.

(78) Zhang, M. N.; Yan, Y. M.; Gong, K. P.; Mao, L. Q.; Guo, Z. X.; Chen, Y. *Langmuir* **2004**, *20*, 8781–8785.

(79) Park, Y. T.; Ham, A. Y.; Yang, Y. H.; Grunlan, J. C. *RSC Adv.* **2011**, *1*, 662–671.

(80) Kovtyukhova, N. L.; Mallouk, T. E. *Adv. Mater.* **2005**, *17*, 187–192.

(81) Agrios, A. G.; Cesar, I.; Comte, P.; Nazeeruddin, M. K.; Gratzel, M. *Chem. Mater.* **2006**, *18*, 5395–5397.

(82) Park, Y. T.; Grunlan, J. C. *Electrochim. Acta* **2010**, *55*, 3257–3267.

(83) Lange, J.; Wyser, Y. *Packag. Technol. Sci.* **2003**, *16*, 149–158.

(84) Sperling, L. H., *Introduction to Physical Polymer Science*; John Wiley & Sons: Hoboken, New Jersey, USA, 2006.

(85) Hanlon, J. F.; Kelsey, R. J.; Forcinio, H. E. Handbook of Package Engineering., Chart or Table, 1998.

(86) Coles, R.; Kirwan, M., *Food and Beverage Packaging Technology*; Wiley-Blackwell: Hoboken, NJ, 2011.

(87) Scopece, P.; Viaro, A.; Sulcis, R.; Kulyk, I.; Patelli, A.; Guglielmi, M. *Plasma Processes Polym.* **2009**, *6*, S705–S710.

(88) Walther, M.; Heming, M.; Spallek, M. *Surf. Coat. Technol.* **1996**, *80*, 200–202.

(89) Sobrinho, A. S. D.; Latreche, M.; Czeremuszkin, G.; Klemberg-Sapieha, J. E.; Wertheimer, M. R. *J. Vac. Sci. Technol., A* **1998**, *16*, 3190–3198.

(90) Faisant, J. B.; Ait-Kadi, A.; Bousmina, M.; Deschenes, L. *Polymer* **1998**, *39*, 533–545.

(91) Turcott, E.; Nguyen, K. T.; Garcia-Rejon, A. *Polym. Eng. Sci.* **2001**, *41*, 603–617.

(92) Triantafyllidis, K. S.; LeBaron, P. C.; Park, I.; Pinnavaia, T. J. *Chem. Mater.* **2006**, *18*, 4393–4398.

(93) Bird, R. B.; Stewart, W. E.; Lightfoot, E. N., *Transport Phenomena*, 2nd. Ed.; J. Wiley: New York, 2002.

(94) Malykh, O. V.; Golub, A. Y.; Teplyakov, V. V. *Adv. Colloid Interface Sci.* **2011**, *164*, 89–99.

(95) Thomas, S.; Joseph, K.; Malhotra, S. K., *Polymer Composites, Nanocomposites*; John Wiley & Sons: Somerset, NJ, 2013.

(96) Wong, M.; Ishige, R.; White, K. L.; Li, P.; Kim, D.; Krishnamoorti, R.; Gunther, R.; Higuchi, T.; Jinnai, H.; Takahara, A.; Nishimura, R.; Sue, H. J. *Nat. Commun.* **2014**, *5*.

(97) Sharma, A.; Tripathi, B.; Vijay, Y. K. *J. Membr. Sci.* **2010**, *361*, 89–95.

(98) Hagen, D. A.; Foster, B.; Stevens, B.; Grunlan, J. C. *ACS Macro Lett.* **2014**, *3*, 663–666.

(99) Stevens, B.; Dessiatova, E.; Hagen, D. A.; Todd, A. D.; Bielawski, C. W.; Grunlan, J. C. *ACS Appl. Mater. Interfaces* **2014**, *6*, 9942–9945.

(100) Nielsen, L. E. *J. Macromol. Sci., Part A: Pure Appl. Chem.* **1967**, *1*, 929–942.

(101) Sun, L. Y.; Boo, W. J.; Clearfield, A.; Sue, H. J.; Pham, H. Q. *J. Membr. Sci.* **2008**, *318*, 129–136.

(102) Cussler, E. L.; Hughes, S. E.; Ward, W. J.; Aris, R. *J. Membr. Sci.* **1988**, *38*, 161–174.

(103) Lape, N. K.; Nuxoll, E. E.; Cussler, E. L. *J. Membr. Sci.* **2004**, *236*, 29–37.

(104) DeRocher, J. P.; Gettelfinger, B. T.; Wang, J. S.; Nuxoll, E. E.; Cussler, E. L. *J. Membr. Sci.* **2005**, *254*, 21–30.

(105) Bharadwaj, R. K. *Macromolecules* **2001**, *34*, 9189–9192.

(106) Fredrickson, G. H.; Bicerano, J. *J. Chem. Phys.* **1999**, *110*, 2181–2188.

(107) Gusev, A. A.; Lusti, H. R. *Adv. Mater.* **2001**, *13*, 1641–1643.

(108) Brodie, B. C. *Philos. Trans. R. Soc. London* **1859**, *149*, 249–259.

(109) Selvig, W. A.; Rabbertz, W. C. *Trans. Am. Electrochem. Soc.* **1921**, *37*, 122–154.

(110) Berthelot, M. *Ann. Chim. Phys.* **1870**, *259*, 392–427.

(111) Staudenmaier, L. *Ber. Dtsch. Chem. Ges.* **1899**, *32*, 1394–1399.

(112) Charpy, G. *C. R. Hebd. Seances Acad. Sci.* **1909**, *148*, 920–923.

(113) Balbiano, M. L. *Bull. Soc. Chim. Fr.* **1916**, *19*, 191–203.

(114) Hummers, W. S.; Offeman, R. E. *J. Am. Chem. Soc.* **1958**, *80*, 1339–1339.

(115) Kovtyukhova, N. I.; Ollivier, P. J.; Martin, B. R.; Mallouk, T. E.; Chizhik, S. A.; Buzaneva, E. V.; Gorchinskiy, A. D. *Chem. Mater.* **1999**, *11*, 771–778.

(116) Marcano, D. C.; Kosynkin, D. V.; Berlin, J. M.; Sinitskii, A.; Sun, Z. Z.; Slesarev, A.; Alemany, L. B.; Lu, W.; Tour, J. M. *ACS Nano* **2010**, *4*, 4806–4814.

(117) Dreyer, D. R.; Park, S.; Bielawski, C. W.; Ruoff, R. S. *Chem. Soc. Rev.* **2010**, *39*, 228–240.

(118) Szabo, T.; Berkesi, O.; Forgo, P.; Josepovits, K.; Sanakis, Y.; Petridis, D.; Dekany, I. *Chem. Mater.* **2006**, *18*, 2740–2749.

(119) Hofmann, U.; Holst, R. *Ber. Dtsch. Chem. Ges. B* **1939**, *72*, 754–771.

(120) Ruess, G. *Monatsh. Chem.* **1947**, *76*, 381–417.

(121) Scholz, W.; Boehm, H. P. *Z. Anorg. Allg. Chem.* **1969**, *369*, 327–340.

(122) Lerf, A.; He, H. Y.; Riedl, T.; Forster, M.; Klinowski, J. *Solid State Ionics* **1997**, *101*, 857–862.

(123) He, H. Y.; Riedl, T.; Lerf, A.; Klinowski, J. *J. Phys. Chem.* **1996**, *100*, 19954–19958.

(124) Lerf, A.; He, H. Y.; Forster, M.; Klinowski, J. *J. Phys. Chem. B* **1998**, *102*, 4477–4482.

(125) He, H. Y.; Klinowski, J.; Forster, M.; Lerf, A. *Chem. Phys. Lett.* **1998**, *287*, 53–56.

(126) Park, S.; An, J.; Potts, J. R.; Velamakanni, A.; Murali, S.; Ruoff, R. S. *Carbon* **2011**, *49*, 3019–3023.

(127) Novoselov, K. S.; Geim, A. K.; Morozov, S. V.; Jiang, D.; Zhang, Y.; Dubonos, S. V.; Grigorieva, I. V.; Firsov, A. A. *Science* **2004**, *306*, 666–669.

(128) Novoselov, K. S.; Geim, A. K.; Morozov, S. V.; Jiang, D.; Katsnelson, M. I.; Grigorieva, I. V.; Dubonos, S. V.; Firsov, A. A. *Nature* **2005**, *438*, 197–200.

(129) Cote, L. J.; Kim, F.; Huang, J. X. *J. Am. Chem. Soc.* **2009**, *131*, 1043–1049.

(130) Watcharotone, S.; Dikin, D. A.; Stankovich, S.; Piner, R.; Jung, I.; Dommett, G. H. B.; Evmenenko, G.; Wu, S. E.; Chen, S. F.; Liu, C. P.; Nguyen, S. T.; Ruoff, R. S. *Nano Lett.* **2007**, *7*, 1888–1892.

(131) Wakabayashi, K.; Pierre, C.; Dikin, D. A.; Ruoff, R. S.; Ramanathan, T.; Brinson, L. C.; Torkelson, J. M. *Macromolecules* **2008**, *41*, 1905–1908.

(132) Yu, A. P.; Ramesh, P.; Itkis, M. E.; Bekyarova, E.; Haddon, R. C. *J. Phys. Chem. C* **2007**, *111*, 7565–7569.

(133) Cote, L. J.; Cruz-Silva, R.; Huang, J. X. *J. Am. Chem. Soc.* **2009**, *131*, 11027–11032.

(134) Williams, G.; Seger, B.; Kamat, P. V. *ACS Nano* **2008**, *2*, 1487–1491.

(135) Stankovich, S.; Piner, R. D.; Nguyen, S. T.; Ruoff, R. S. *Carbon* **2006**, *44*, 3342–3347.

(136) Fernandez-Merino, M. J.; Guardia, L.; Paredes, J. I.; Villar-Rodil, S.; Solis-Fernandez, P.; Martinez-Alonso, A.; Tascon, J. M. D. *J. Phys. Chem. C* **2010**, *114*, 6426–6432.

(137) Pei, S. F.; Zhao, J. P.; Du, J. H.; Ren, W. C.; Cheng, H. M. *Carbon* **2010**, *48*, 4466–4474.

(138) Pei, S. F.; Cheng, H. M. *Carbon* **2012**, *50*, 3210–3228.

(139) Stevens, B. E.; Odenborg, P. K.; Priolo, M. A.; Grunlan, J. C. *J. Polym. Sci., Part B: Polym. Phys.* **2014**, *52*, 1153–1156.

(140) Inagaki, N.; Tasaka, S.; Hiramatsu, H. *J. Appl. Polym. Sci.* **1999**, *71*, 2091–2100.

(141) Jang, W. S.; Rawson, I.; Grunlan, J. C. *Thin Solid Films* **2008**, *516*, 4819–4825.

(142) Lachewsky, A.; Mallwitz, F.; Baussard, J. F.; Cochin, D.; Fischer, P.; Jiwan, J. L. H.; Wischerhoff, E. *Macromol. Symp.* **2004**, *211*, 135–155.

(143) Olugebefola, S. C.; Ryu, S. W.; Nolte, A. J.; Rubner, M. F.; Mayes, A. M. *Langmuir* **2006**, *22*, 5958–5962.

(144) Lee, S.; Duhamel, J. *Macromolecules* **1998**, *31*, 9193–9200.

(145) Yip, J.; Duhamel, J.; Qiu, X. P.; Winnik, F. M. *Macromolecules* **2011**, *44*, 5363–5372.

(146) Winnik, M. A.; Bystryak, S. M.; Liu, Z.; Siddiqui, J. *Macromolecules* **1998**, *31*, 6855–6864.

(147) Cao, T.; Fasulo, P. D.; Rodgers, W. R. *Appl. Clay Sci.* **2010**, *49*, 21–28.

(148) Owens, D. K. *J. Appl. Polym. Sci.* **1975**, *19*, 265–271.

(149) Gamboa, D.; Priolo, M. A.; Ham, A.; Grunlan, J. C. *Rev. Sci. Instrum.* **2010**, *81*, 036103.

(150) Podsiadlo, P.; Michel, M.; Lee, J.; Verploegen, E.; Kam, N. W. S.; Ball, V.; Lee, J.; Qi, Y.; Hart, A. J.; Hammond, P. T.; Kotov, N. A. *Nano Lett.* **2008**, *8*, 1762–1770.

(151) Lavalle, P.; Gergely, C.; Cuisinier, F. J. G.; Decher, G.; Schaaf, P.; Voegel, J. C.; Picart, C. *Macromolecules* **2002**, *35*, 4458–4465.

(152) Kim, Y. H.; Lee, Y. M.; Park, J.; Ko, M. J.; Park, J. H.; Jung, W.; Yoo, P. J. *Langmuir* **2010**, *26*, 17756–17763.

(153) Dubas, S. T.; Farhat, T. R.; Schlenoff, J. B. *J. Am. Chem. Soc.* **2001**, *123*, 5368–5369.

(154) Sukhishvili, S. A.; Granick, S. *J. Am. Chem. Soc.* **2000**, *122*, 9550–9551.

(155) Chen, J. T.; Fu, Y. J.; An, Q. F.; Lo, S. C.; Huang, S. H.; Hung, W. S.; Hu, C. C.; Lee, K. R.; Lai, J. Y. *Nanoscale* **2013**, *5*, 9081–9088.

(156) Svagan, A. J.; Akesson, A.; Cardenas, M.; Bulut, S.; Knudsen, J. C.; Risbo, J.; Plackett, D. *Biomacromolecules* **2012**, *13*, 397–405.

(157) Lewis, J. S.; Weaver, M. S. *IEEE J. Sel. Top. Quantum Electron.* **2004**, *10*, 45–57.

(158) Li, D.; Muller, M. B.; Gilje, S.; Kaner, R. B.; Wallace, G. G. *Nat. Nanotechnol.* **2008**, *3*, 101–105.

(159) Bunch, J. S.; Verbridge, S. S.; Alden, J. S.; van der Zande, A. M.; Parpia, J. M.; Craighead, H. G.; McEuen, P. L. *Nano Lett.* **2008**, *8*, 2458–2462.

(160) El-Kady, M. F.; Strong, V.; Dubin, S.; Kaner, R. B. *Science* **2012**, *335*, 1326–1330.

(161) Eda, G.; Fanchini, G.; Chhowalla, M. *Nat. Nanotechnol.* **2008**, *3*, 270–274.

(162) Zhu, J. Y.; He, J. H. *Nanoscale* **2012**, *4*, 3558–3566.

(163) Brunauer, S.; Emmett, P. H.; Teller, E. *J. Am. Chem. Soc.* **1938**, *60*, 309–319.

(164) Wong, J. E.; Rehfeldt, F.; Hanni, P.; Tanaka, M.; Klitzing, R. V. *Macromolecules* **2004**, *37*, 7285–7289.

(165) Nolte, A. J.; Treat, N. D.; Cohen, R. E.; Rubner, M. F. *Macromolecules* **2008**, *41*, 5793–5798.

(166) Cho, C. Y.; Valverde, L.; Ozin, G. A.; Zacharia, N. S. *Langmuir* **2010**, *26*, 13637–13643.

(167) Campbell, C. J.; Smoukov, S. K.; Bishop, K. J. M.; Grzybowski, B. A. *Langmuir* **2005**, *21*, 2637–2640.

(168) Campbell, C. J.; Fialkowski, M.; Bishop, K. J. M.; Grzybowski, B. A. *Langmuir* **2009**, *25*, 9–12.

(169) Choi, J.; Rubner, M. F. *Macromolecules* **2005**, *38*, 116–124.

(170) Shih, C. J.; Lin, S. C.; Sharma, R.; Strano, M. S.; Blankschtein, D. *Langmuir* **2012**, *28*, 235–241.

(171) Konkena, B.; Vasudevan, S. *J. Phys. Chem. Lett.* **2012**, *3*, 867–872.

(172) Henry, B. M.; Norenberg, H.; Dinelli, F.; Grovenor, C. R. M.; Briggs, G. A. D.; Tsukahara, Y.; Miyamoto, T. *Chem. Eng. Technol.* **1999**, *22*, 1010–1011.

(173) Lee, D. W.; Kim, T.; Lee, M. *Chem. Commun.* **2011**, *47*, 8259–8261.

(174) Liu, J. Q.; Yang, W. R.; Tao, L.; Li, D.; Boyer, C.; Davis, T. P. *J. Polym. Sci., Part A: Polym. Chem.* **2010**, *48*, 425–433.

(175) Su, Q.; Pang, S. P.; Alijani, V.; Li, C.; Feng, X. L.; Mullen, K. *Adv. Mater.* **2009**, *21*, 3191–3195.